Prepared for publication at the Fall Creek Falls Meeting on Heavy-Ion Collisions, Pikeville, Tenn., June 13-17, 1977

CONF-770602--1

HEAVY ION REACTIONS - AN EXPERIMENTAL VISTA*

R. G. Stokstad

Oak Ridge National Laboratory
Oak Ridge, Tennessee 37830

ABSTRACT

Examples of recent experiments in the areas of fusion and deep-inelastic scattering are presented and discussed. Emphasis is placed on the importance of individual nucleons in the fusion process, the effects of high angular momentum, and our understanding of compound nuclear decay. Experiments on deep inelastic scattering are entering a new stage in which important parameters of the reaction mechanism are now open to investigation. Primarily through coincidence measurements, direct information on the angular momentum transferred in a collision and on the time scale of decay is being obtained.

I. INTRODUCTION

The rate at which our understanding of heavy-ion reaction mechanisms increases is astounding and exciting. It would be impossible to keep up with, let alone contribute effectively to, this rapidly developing field without the personal communication and interaction provided by topical conferences.

This meeting at Fall Creek Falls will emphasize, in the words of our organizing committee, "theoretical descriptions." I note however that about half of the scheduled talks are to be delivered by experimentalists. This recognizes, I believe, that we are ultimately concerned with theoretical descriptions of experimental data. If the necessary data do not exist, then we must acquire them. (The completion of GSI, the scheduled upgrading of the Bevelac, and the accelerator projects at Daresbury, Caen and Oak Ridge represent a strong commitment to this.) If new measurements exist, but the theoretical descriptions have not been brought to the level of a quantitative comparison, then this is also a challenge to be met. The interfacing of these two complementary approaches to "understanding" is one of the reasons why we are here. The talks you will hear from my experimentalist colleagues in the coming sessions will provide a broad view of what is new and exciting in current experimental work. In a real sense, it is the sum of all these presentations which will constitute the "vista" provided by experimental studies of heavy-ion collisions.

* Work supported by U.S. Energy Research and Development Administration under contract with the Union Carbide Corporation.

NOTICE
This report was prepared as an account of work sponsored by the United States Government. Neither the United States nor the United States Energy Research and Development Administration, nor any of their employees, nor any of their contractors, subcontractors, or their employees, makes any warranty, express or implied, or assumes any legal liability or responsibility for the accuracy, completeness or usefulness of any information, apparatus, product or process disclosed, or represents that its use would not infringe privately owned rights.

DISTRIBUTION OF THIS DOCUMENT IS UNLIMITED

By acceptance of this article, the publisher and recipient acknowledges the U.S. Government's right to retain a non-exclusive, royalty-free license in and to any copyright covering the article.

MASTER

I have selected a number of experiments which illustrate the kinds of information now being obtained in the areas of fusion and deep inelastic scattering. As you will see, these experiments involve reactions throughout the periodic table and bombarding energies ranging over more than two orders of magnitude.

Much of the data you will see is not yet published, and I refer you to the acknowledgements for recognition of those who have very kindly communicated their results prior to publication.

Figure 1 outlines the physics I wish to cover. I have opted to mention a large number of experiments, describing only their essential features and results, rather than concentrating on only a few. (Regrettably, it is not possible to describe some of the elegant and sophisticated experimental techniques which have made some of these results possible.)

FUSION

MICROSCOPIC ASPECTS

ANGULAR MOMENTUM LIMITATIONS

COMPOUND NUCLEUS DECAY

DEEP INELASTIC SCATTERING

ALIGNMENT AND ANGULAR MOMENTUM TRANSFER

TIME SCALE AND MECHANISMS FOR DECAY

FIG. 1. Topics to be discussed.

Section IV gives a summary which attempts to tie this altogether.

II. FUSION

A. Microscopic Aspects

Even though the fundamental constituents of the nucleus are protons and neutrons, surprisingly little is known about the importance of individual nucleons in processes such as fusion. Perhaps this should be taken as an indication that the effects of individual nucleonic motion are not of importance in determining the fusion cross section, and that macroscopic and collective variables are all that matter. Macroscopic properties (radii, deformation, potentials, etc.) may be derived from microscopic models, however, and such calculations provide a motivation for the experiments I will discuss. The two-center shell model calculations of Glas and Mosel (GL 74), for example, suggest that the fusion cross section might depend on which shell model orbitals are occupied, and hence on the valence nucleons of the target and projectile. Figure 2 shows the energies of shell model configurations for the two-center ^{16}O-^{16}O system as a function of the separation between the centers of the oscillator wells. Nuclear interactions leading to fusion occur at level crossings and are estimated with the Landau-Zener approximation. If we argue that the

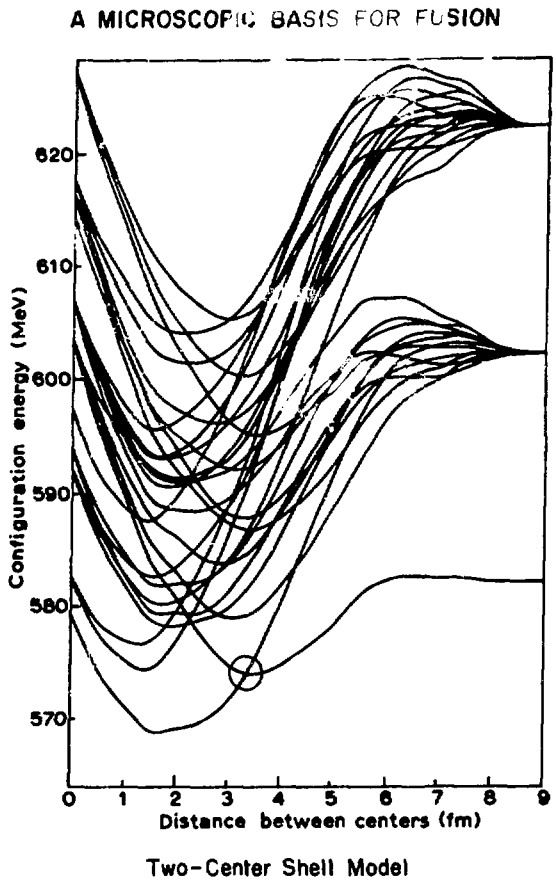

FIG. 2. Configuration energies calculated with the two-center shell model as a function of the separation of the centers. At distances less than 3.4 fm, the lowest energy configuration is the ^{32}S ground state, at larger distances it is the ^{16}O-^{16}O ground state. Fusion is initiated at such level crossings (Gl 74,76).

first level crossing (circled in Fig. 2) in some way determines a critical radius for fusion, then changes in the fusion cross section might be observed as individual nucleons are added or subtracted from the target or projectile. To be considered as evidence for microscopic processes in fusion, we require that these changes be in addition to those expected on the basis of changes in Coulomb barrier or macroscopic "$A^{1/3}$-type" changes in radius.

Recent experimental results on fusion cross sections have much to say on this question. Figure 3 illustrates the characteristic energy regions for fusion. This one-dimensional classification is valid for relatively light heavy-ion systems for which the dynamical path for fusion lies inside the saddle point for fission (Mö 76). In region 1, for small values of σ_{fus}, penetration of the Coulomb barrier is the mechanism governing the order of magnitude of the cross section. In region 2, direct reactions begin to compete, and σ_{fus} can experience a maximum value and then decrease slowly. We shall consider each of these regions in turn but will postpone the discussion of the third region to Section IIB.

The high currents and availability of low energy Van de Graaff accelerators has enabled the measurement of fusion cross sections covering the extreme range of tens of nanobarns to ~ 1 barn. Recently, systematic studies of a large number of systems have become available (St 76, Cu 76, Hi 76, 77b). Typical experimental results are shown in Fig. 4 for the $^{12}C + {}^{13}C$ system (Da 76b). The fusion cross section is

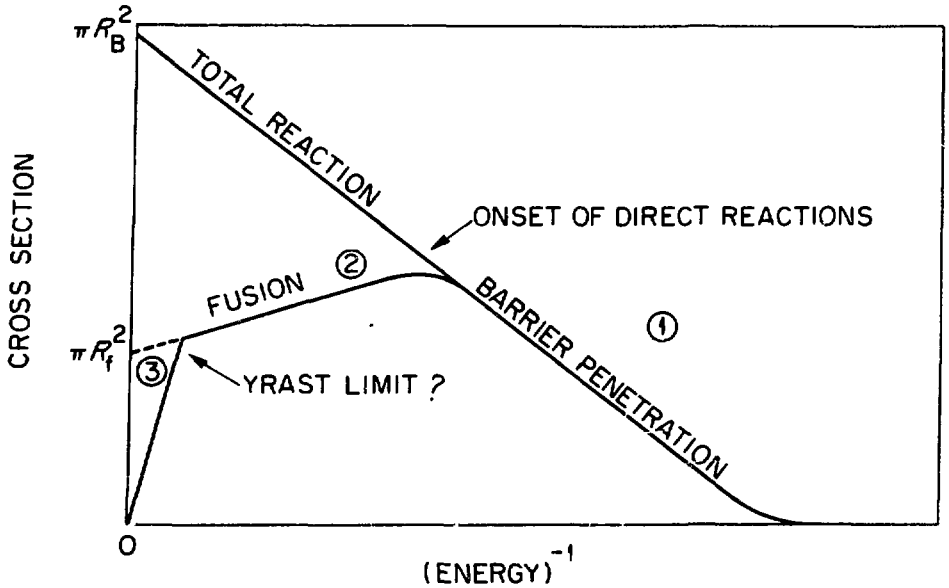

Characteristic Energy Regions for Fusion.

FIG. 3. Schematic representation of the fusion cross sections and total reaction cross section as a function of the reciprocal of the bombarding energy.

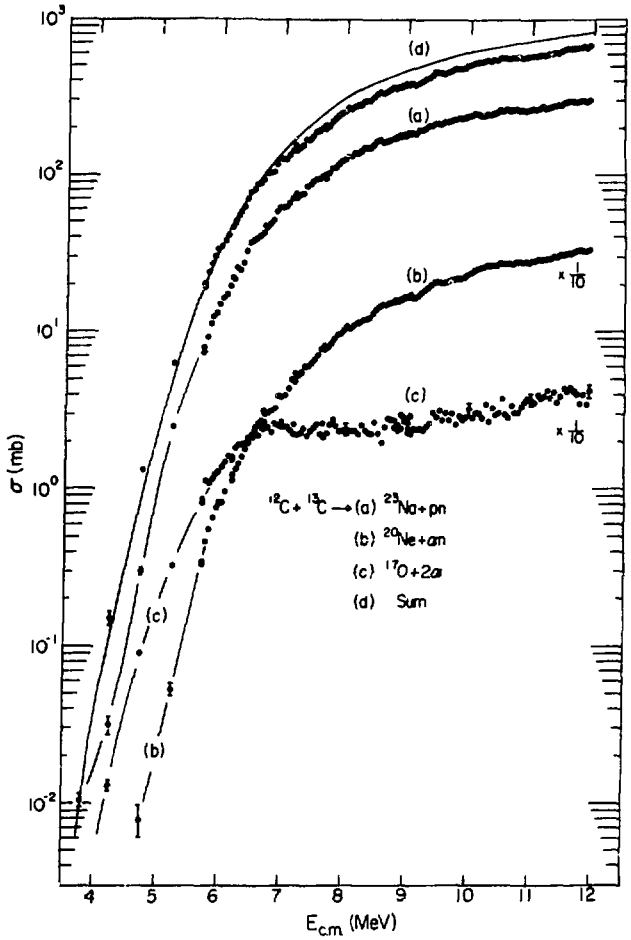

FIG. 4. Energy dependence of evaporation-residue cross sections for ^{12}C + ^{13}C at sub-Coulomb bombarding energies. The full drawn curve is an optical model calculation for the fusion cross section, coupled with a statistical model calculation for branching to the observed residues (Da 76b).

deduced from the observation of discrete γ-ray lines in the residue of the compound nucleus. The full curve which is compared with the sum of the cross sections to all bound states in ^{23}Na, ^{20}Ne and ^{17}O represents the effect of barrier penetration as given by an optical model calculation of the entrance channel transmission coefficients and a statistical model calculation of the decay of the compound nucleus. It is the deviation of the cross section from this prediction which is of interest. In the following presentation of the experimental results, the total fusion cross section was first deduced from experiment and was then divided by the cross section calculated with the optical model using a single set of parameters.* The energy scale in the center of mass has been shifted by an amount $E_{Coul} = \frac{Z_1 Z_2 e^2}{R}$ where $R = 1.7(A_1^{1/3} + A_2^{1/3})$ fm.

Figures 5 and 6 present the quantity $R = \sigma_{fusion}/\sigma_{opt.mod.}$ vs. $E_{c.m.} - E_{Coul}$ for 14 heavy-ion systems with projectiles and targets in the 1p shell. In Fig. 5 we see that the cross sections involving the isotopes of ^{10}B and ^{11}B are all reproduced very well by the "standard" optical model. There is perhaps a small decrease in R(E) at the lower energies for $^{14}N + {}^{10}B$, but it is not marked. Given our operational definition above, one would not cite any evidence for microscopic effects based on a comparison of the lower six excitation functions shown in Fig. 5. The energy dependence for $^{16}O + {}^{9}Be$ (Sw 77b), however is quite different, with R rising by a factor of 2 from the lowest to the highest energy. It is interesting to note that this system, as does $^{12}C + {}^{9}Be$ (Cu 77), has a direct reaction channel involving neutron transfer to the heavy partner which far exceeds the fusion cross section at low energies. In Fig. 6 the values of R for systems involving projectiles and targets both with masses ≥ 12 are shown. The difference between Fig. 5 and Fig. 6 is striking. A general feature for the systems in Fig. 6 is that R decreases at lower energies even though the detailed behavior in all systems is by no means identical. (The narrow resonances in $^{12}C + {}^{12}C$ and to a lesser extent in $^{16}O + {}^{12}C$ are noteworthy, but that is another story; we are concerned here with the energy-averaged behavior of the data.) The average energy dependence of R for $^{16}O + {}^{14}N$ is quite different from that of $^{16}O + {}^{16}O$. The systems $^{14}N + {}^{12}C$, $^{13}C + {}^{12}C$ and $^{12}C + {}^{12}C$ are all different. The differences referred to can be quite large also, up to factors of two.

The message of Figs. 5 and 6 is simply stated. The addition or subtraction of one or two nucleons from the projectile or target can

---

*V = 50 MeV, W = 10 MeV, r_0 = 1.27 fm, a = 0.4 fm; matching radius = 15a + the larger of R or D, where R is the nuclear radius and D is the distance of closest approach.

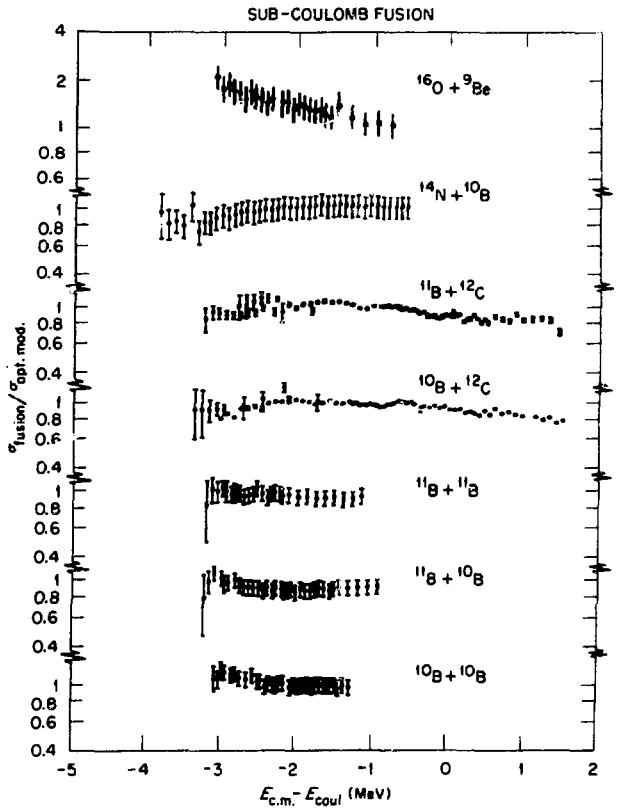

FIG. 5. The ratio of measured fusion cross sections to a standard optical model prediction for sub-Coulomb energies. The energy scale in each case has been shifted such that 0 MeV corresponds to $E_{c.m.} = Z_1Z_2e^2/R$ MeV where $R = 1.7(A_1^{1/3} + A_2^{1/3})$ fm. The experimental data are taken from: $^{10}B + ^{10}B$, $^{11}B + ^{10}B$, $^{11}B + ^{11}B$ (Hi 76); $^{10}B + ^{12}C$, $^{11}B + ^{12}C$ (Da 76, Hi 77b); $^{14}N + ^{10}B$ (Hi 77b); $^{16}O + ^{9}Be$ (Sw 77b).

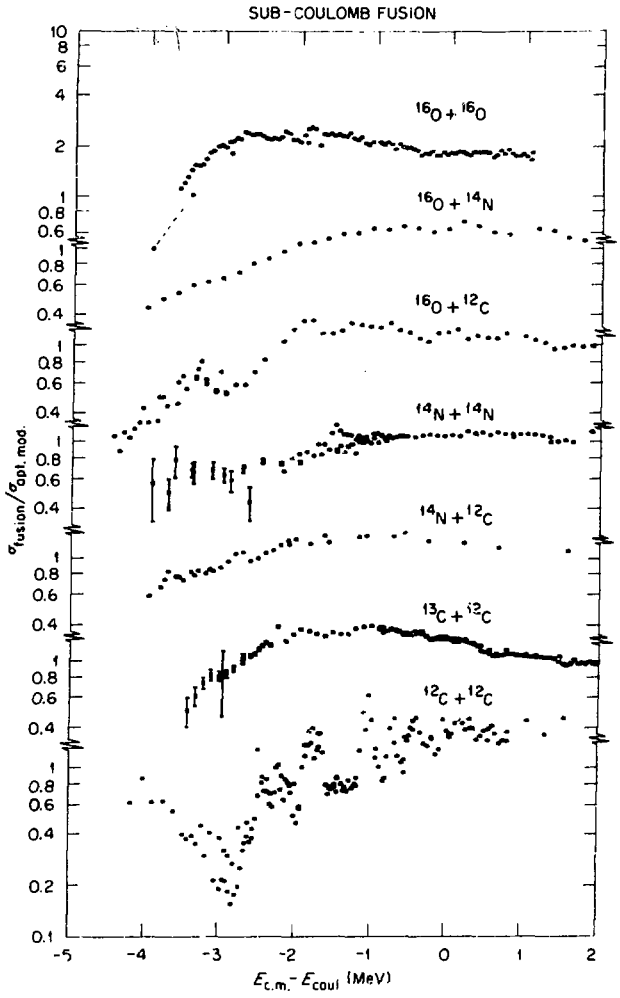

FIG. 6. The ratio of measured fusion cross sections to a standard optical model prediction for sub-Coulomb energies. The energy scale in each case has been shifted such that 0 MeV corresponds to $E_{c.m.} = Z_1Z_2e^2/R$ MeV where $R = 1.7(A_1^{1/3} + A_2^{1/3})$ fm. The experimental data are taken from: $^{12}C + ^{12}C$ (Ma 73); $^{12}C + ^{13}C$ (Da 76b); $^{14}N + ^{12}C$, $^{14}N + ^{16}O$ (Sw 77a); $^{12}C + ^{16}O$ (Cu 76); $^{14}N + ^{14}N$ (Sw 76c); $^{16}O + ^{16}O$ (Sp 74).

have a profound effect upon the energy dependence for fusion. This is a strong indication that the valence nucleons play an important role in the mechanisms leading to fusion. At present there is no qualitative or quantitative explanation for the disparate results shown in Figs. 5 and 6. Quantitative microscopic calculations for comparison with these data are needed. In one case (Wi 77), a folding model calculation of the real potential for the different systems has been made. The imaginary potential was taken to be a Woods Saxon with W = 10 MeV, r_0 = 1.27 fm, and a = 0.4 fm. This procedure yields values of $R = \sigma_{\text{folded potential}}/\sigma_{\text{opt.mod.}} \simeq 1$ for all reactions. Thus, the microscopic effects may well be contained in the imaginary potential.

The real interaction potentials for $^{12}C + ^{12}C$ and $^{16}O + ^{16}O$ have been calculated in the two-center shell model (Pr 70) and in the TDHF approximation (Ma 76, Ko 77). Generally, the calculations now available are for closed shell systems or even-even nuclei and comparisons with the low energy data has not been extensive. Recently, a macroscopic treatment of the potentials has been presented (Ar 76). Phenomenological comparisons with the data for the α-conjugate systems are found in refs. Ch 77, Mi 72 and Fo 75.

In summary, the experimental results shown in Figs. 5 and 6 together with those to be discussed next provide an excellent opportunity for testing microscopic calculations of the fusion process.

The value of σ_{fus} in region 2 of Fig. 3, the energy region over the Coulomb barrier, provides another opportunity for observing the effects of individual nucleons on the fusion process. The experimental technique used in this region differs in that the residues of compound nucleus decay are observed directly with a ΔE-E counter telescope. This technique can be sufficiently precise that the rather small changes in the fusion cross section associated with the $A^{1/3}$ dependence of the nuclear radius can be observed, even with the addition of only one nucleon. Figure 7 shows measurements of σ_{fus} for $^{16,17,18}O + ^{27}Al$ just above the Coulomb barrier (Ei 77). The straight lines represent fits to the data using the classical expression $\sigma_{fus} = \pi R_B^2 (1 - \frac{V_B}{E_{c.m.}})$. The small changes (∿ 5-10%) in the fusion cross section in this energy region are consistent with the increase in size of the oxygen nucleus as neutrons are added.

A more dramatic change in behavior of the fusion cross section at energies well above the Coulomb barrier is illustrated in Fig. 8 (Vi 76, Sp 76a,b). When the small resonances in the $^{12}C + ^{16}O$ data are averaged by fitting the data with, e.g., the expression of Glas

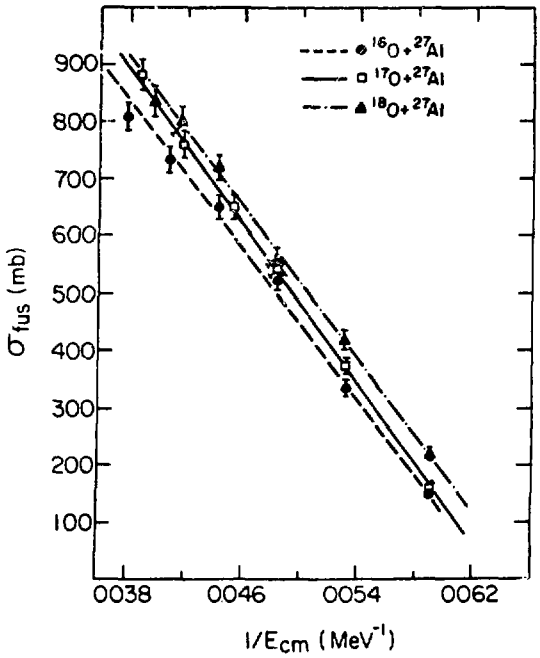

FIG. 7. Fusion cross sections for $^{16,17,18}O + ^{27}Al$ (Ei 77). The straight lines are fits to the data. The differences between the cross sections for the different projectile isotopes reflect in large part the $A^{1/3}$ dependence of the oxygen radius.

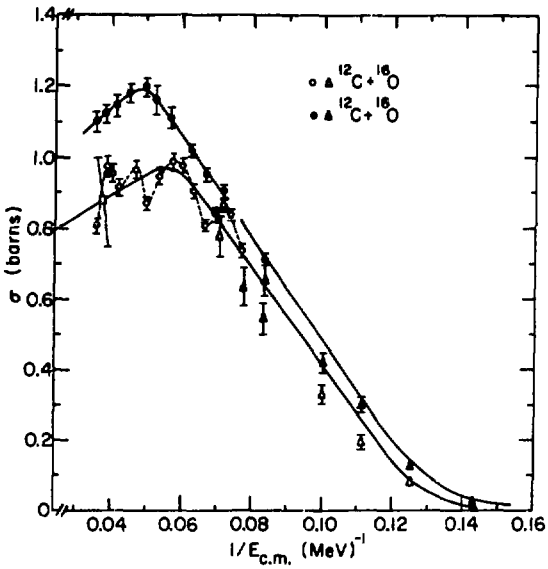

FIG. 8. Fusion cross sections for $^{12}C + ^{16}O$, $^{12}C + ^{18}O$ (Vi 76, Sp 76a, Sp 76b, Ei 77). The curved lines are fits to the data using the formula of Glas and Mosel (Gl 75).

and Mosel (Gl 75), a difference of about 200 mb or 20% in the value of the maximum fusion cross section is noted. (We would expect an increase of $\lesssim$ 5% based on the $A^{1/3}$ change in radius of ^{18}O-^{16}O.) Systematic studies of the value of σ_{fus}(max) in this mass region led to the suggestion that the 200 mb increase was associated with the addition of one or more nucleons in the s-d shell (Sp 76b). The addition of nucleons into a major oscillator shell presumably could cause an abrupt change in the mean-square radius. Figure 9 summarizes the experimental data currently available for the maximum fusion cross section in the region above the Coulomb barrier. The correlation of the abrupt change in the fusion cross section of $\sim$ 200 mb with the introduction of a nucleus in the s-d shell is upset by the recent measurement of the ^{15}N + ^{12}C fusion cross section (Co 76). This value is $\sim$ 15% larger than that of ^{14}N + ^{12}C and much closer to the value prevalent when one of the reaction partners is in the s-d shell.

It appears that the manner in which valence nucleons affect the magnitude and the energy dependence of the fusion cross section for these light heavy ions is yet to be understood. Perhaps the role played by these nucleons is complex - indeed, the complexity of Fig. 2 suggests this - and coupling to direct reactions or collective modes of motion may be important (Pe 76).

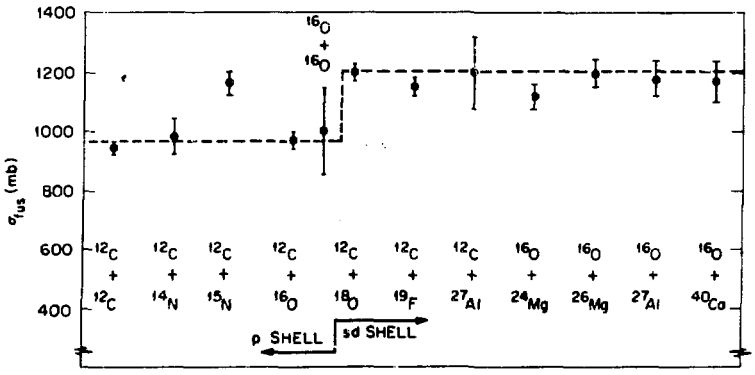

FIG. 9. Measured values of the maximum fusion cross section for different systems. Cases in which both the projectile and target are in the p shell are in the left hand portion of the figure, as indicated. The apparent systematics $\sigma_{fus} \sim$ 1000 mb for p shell nuclei and $\sigma_{fus} \sim$ 1200 mb for s-d shell targets, is upset by the large value of σ_{fus} for ^{15}N + ^{12}C. The experimental data are taken from: ^{12}C + ^{12}C, ^{12}C + ^{16}O, ^{18}O + ^{12}C, ^{12}C + ^{19}F, ^{16}O + $^{24,26}Mg$ (Vi 76, Sp 76a, Sp 76b, Sc 77), ^{12}C + ^{14}N (Co 76, St 77, Sc 77), ^{12}C + ^{15}N (Co 76, Sc 77); ^{12}C + ^{27}Al (Be 76), ^{16}O + ^{16}O (We 76).

B. Angular Momentum Limitations

A macroscopic view of the fusion process enables an "understanding" of the gross behavior of σ_{fus} in regions (1) and (2) (Fig. 3) in terms of a barrier. At low energies, it is the Coulomb barrier. At high energies, region 2, it is predominantly the centrifugal barrier. The degree of penetration required for fusion is determined by a hypothetical critical radius (Ga 74, Gl 75) which is nearly equivalent to an energy dependent critical angular momentum (Ba 73). This approach and somewhat more sophisticated one dimensional calculations (Gr 74) have been extremely successful in reproducing experimental data over a wide range of energy and mass for which the dynamical path to fusion lies inside the saddle point for fission. There remains the possibility of an additional limitation on the fusion mechanism, however, which has been harder to detect experimentally. This limit would occur in region 3 of Fig. 2, and is a Yrast limit. That is, the compound nucleus cannot be formed if, at that excitation energy, a state with angular momentum J does not exist. This "absolute" upper limit on the angular momentum is usually calculated with the rotating liquid drop model (Co 74). Previous measurements where the angular momentum introduced at the critical radius approaches that of the liquid drop limit are described in refs. Na 75, Br 76b, and Vi 76.

Results of a recent experiment (St 77) in which both the effect of penetration to a critical radius and, apparently, that of a Yrast limit are present are shown in Fig. 10. At the right hand portion of the figure (low bombarding energies) the beginning of the drop in σ_{fus} is just on scale. In the region $0.012 \leq E^{-1} \leq 0.05$ ($180 \geq E \geq 43$ MeV), σ_{fus} varies linearly with E^{-1}, consistent with penetration to a critical radius. At the highest bombarding energy, $E_{^{14}N} = 248$ MeV, a significant decrease in the value of σ_{fus} of about 200 mb is observed.

Two dimensional TDHF calculations (Ma 77) have been performed and compared to these data. The theoretical cross sections for σ_{fus} decrease from about 1150 mb at $E^{-1}_{c.m.} = 0.02$ to 900 mb at $E^{-1}_{c.m.} = 0.009$.

The results of Fig. 10 may be plotted in a different manner by converting σ_{fus} to a critical angular momentum J using the sharp cutoff relation $\sigma_{fus} = \pi \lambda\!\!\!^{-2} (J + 1)^2$ and plotting the results versus excitation energy in ^{26}Al ($E^* = E_{c.m.} + 15$ MeV separation energy). The maximum angular momentum for which fusion occurs is seen to change only very little with excitation energy for the two highest energy data points. The solid vertical line at $J_{max} = 26.6\ \hbar$ represents the prediction of the rotating liquid drop model, which is consistent with the experimental data. The trend of the experimental results in Fig. 11 suggests that the maximum angular momentum which a ^{26}Al

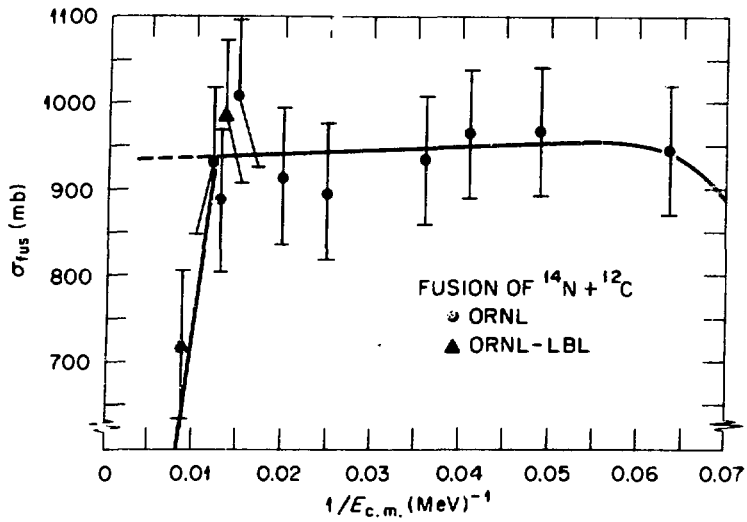

FIG. 10. The fusion cross section for $^{14}N + ^{12}C$ at ^{14}N bombarding energies from 34 MeV to 248 MeV. The solid line for $0.012 \leq E_{c.m.} \leq .05$ is a straight line fit to the data in that region. The solid line for $E_{c.m.} < 0.012$ corresponds to the fusion cross section expected for a Yrast limit of $\sim 27\ \hbar$ (St 77).

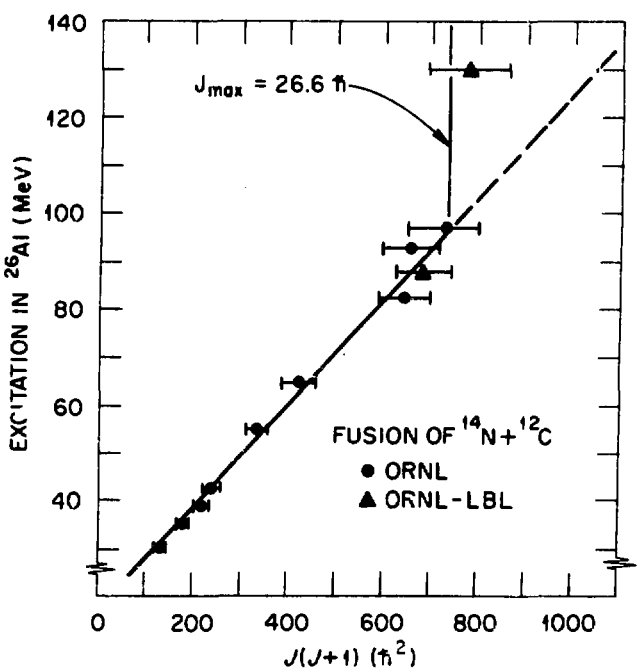

FIG. 11. The critical angular momenta for $^{12}C + ^{14}N$ deduced from the measured values of σ_{fus} using $\sigma_{fus} = \pi\lambda\!\!\!^{-2}(J+1)^2$, (St 77). The angular momentum corresponding to the liquid drop limit (Co 74) $J_{max} = 26.6\ \hbar$, is shown.

compound nucleus may have (at any excitation energy) has been observed and is ∿ 1 ħ/nucleon.

C. Compound Nucleus Decay

Several important properties of the compound nucleus become accessible through the measurement and analysis of the decay products. Such quantities are the temperature, distribution of angular momenta and moments of inertia and the degree of equilibration. Analysis of the reaction products usually involves comparison of the data with the predictions of an evaporation calculation, i.e. a statistical model. Significant progress has been made both in the range and quality of experimental data and the sophistication of the computer codes used for the analysis (Pü 77, Go 77, Hi 77). As an example, the mass distributions obtained from the fusion of ^{19}F and ^{27}Al are shown for four different bombarding energies in Fig. 12 (Pü 77). The experimental data were obtained with a time-of-flight spectrometer as described in ref. Pü 75. The main decay mode leading to several of the residual masses is indicated. The production of lighter residues and the increased importance of multiple α-particle emission as the bombarding energy is increased is immediately apparent. That the increased α-particle emission is associated with higher angular momentum rather than higher excitation energy is illustrated in Fig. 13 in which calculated mass distributions as a function of compound nucleus angular momentum are presented. Thus, the residues corresponding to α-particle emission probe the region of the energy-angular momentum plane nearer the Yrast line of the compound nucleus. Analysis of the relative intensity of these products indicates that the compound nuclei in this mass region and their immediate daughters are quite deformed at high excitation energy and angular momenta (Pü 77, see also St 77).

The mass distribution obtained from the decay of a much heavier system, ^{151}Tb, formed in the reaction ^{65}Cu + ^{86}Kr (716 MeV) is shown in Fig. 14 (Br 76b, Br 76c, Pl 77). An evaporation calculation (Pl 75, Pl 77) reproduces the distribution of residues rather well.

Since a large amount of experimental data on the mass and/or charge distributions of evaporation residues is available it is of interest to examine the systematics of a simple quantity such as the average amount of mass evaporated versus excitation energy. (This has been done for the case of ^{151}Tb, Pl 77). In Fig. 15, results from some 14 different compound systems are shown. The ordinate is $\Delta A = A_{C.N.} - \bar{A}_{residue}$ where A is the average mass of the evaporation residues. In cases where Z-distributions were measured, the conversion to mass was made using the N/Z ratio appropriate for nuclei near the most probable Z-value. Several features of this plot are of interest. Typical values of the excitation energy removed per mass unit range from ∿ 7-12 MeV/amu.

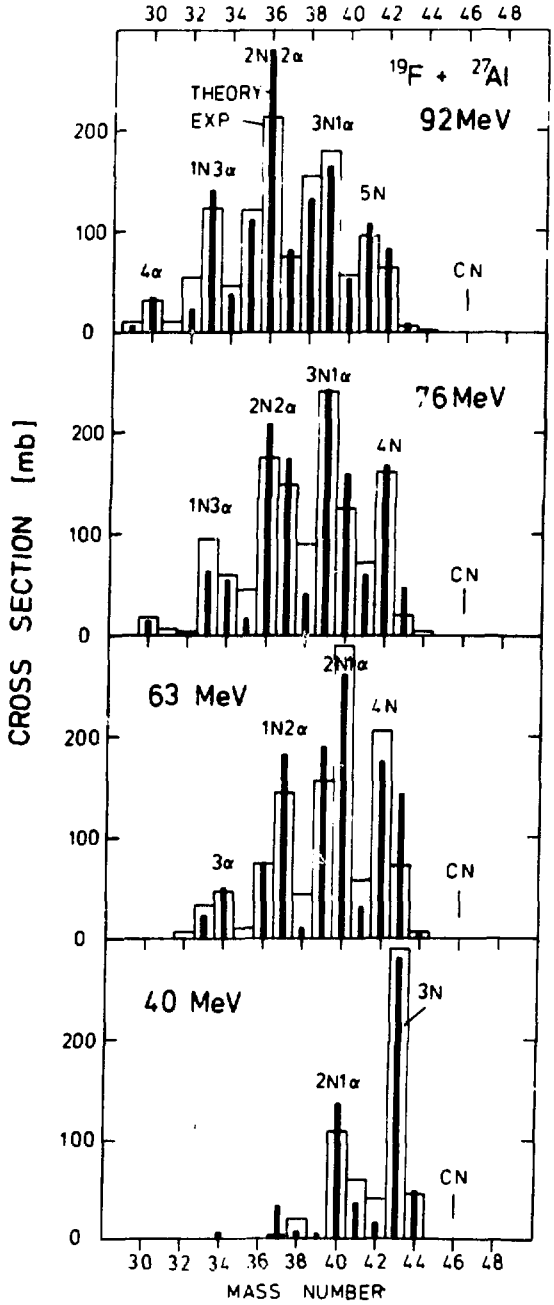

FIG. 12. Measured and predicted mass distributions for the evaporation residues of $^{19}F + ^{27}Al$ (Pü 77).

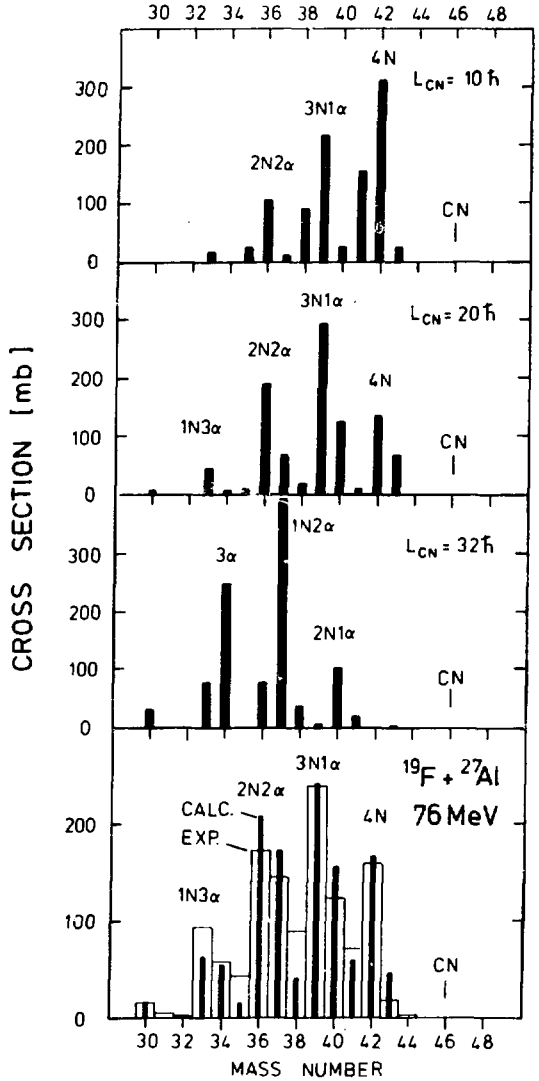

FIG. 13. The predicted distribution of residues for different angular momenta of the compound nucleus (PÜ 77).

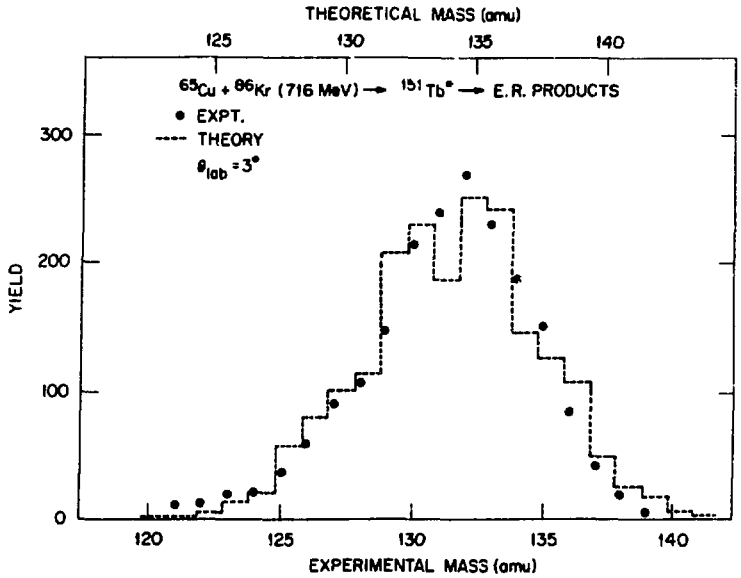

FIG. 14. Measured and predicted mass distributions for the evaporation residue products of ^{151}Tb (Br 76c, Pl 77).

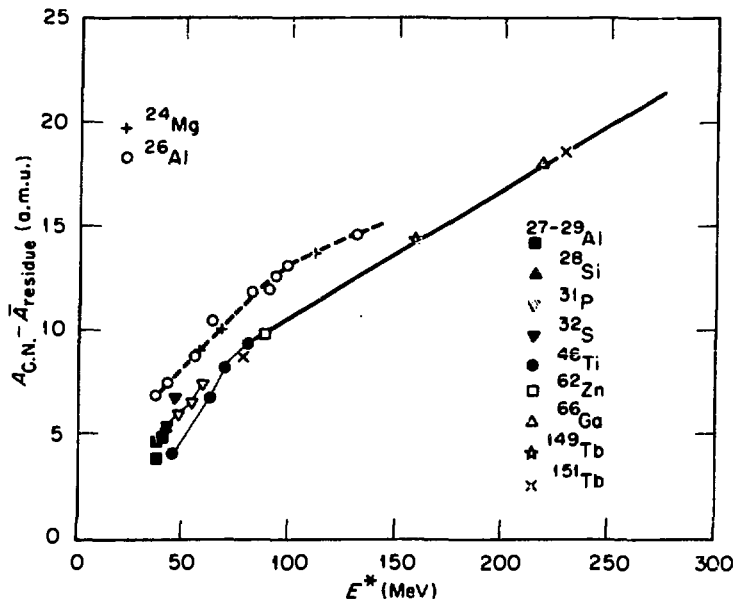

Evaporated Mass vs Compound Excitation.

FIG. 15. The average evaporated mass (in amu) versus compound nucleus excitation energy for a variety of compound nuclei produced in heavy ion reactions. Very light systems evaporate more mass per unit excitation energy than do heavier systems. This can be attributed to the larger angular momenta with which the heavier nuclei are produced. The data are taken from ^{24}Mg (Na 75), ^{26}Al (St 77), $^{27-29}$Al (Co 76b), ^{28}Si (We 76), ^{31}P (Pü 75, Ko 77b), ^{32}S (We 76), ^{46}Ti (Pü 77), ^{62}Zn (Co 77), ^{66}Ga (Na 75), ^{149,151}Tb (Br 76b, Pl 77).

These values are reasonable considering separation energies, temperatures and the fact that α-particles as well as nucleons are emitted. Systematic trends are also evident. The heavier nuclei, e.g. A $\gtrsim$ 40 tend to lie on one curve whereas lighter compound nuclei emit, on the average, more mass per unit excitation energy. There are two reasons why a heavier system should emit fewer particles to remove a given amount of excitation energy. Both reasons are connected with the fact that they are formed (in these heavy ion reactions) with much larger angular momenta. High angular momentum and heavy nuclei favor γ-ray emission which means less mass is evaporated. The main reason, however, is that the removal of angular momentum requires particles to be emitted with energies greater than the sum of the Coulomb repulsion and thermal energies. Since each particle then carries off on the average more energy, fewer particles are emitted in removing a given amount of excitation energy. Statistical model calculations reproduce these trends fairly well.

It appears that, over a wide range of compound nuclear masses, excitation energies, and angular momenta, the decay of the compound nucleus can be adequately explained on the basis of an equilibrated nucleus and statistical decay. This statement has a practical significance which is in addition to the obvious importance of understanding the decay of the compound nucleus. It facilitates the comparison of theoretical calculations of heavy-ion reactions, in which large amounts of energy are converted into excitation of the fragments, to results obtained in the laboratory. The excited reaction products will emit some number of particles before being detected and this must be taken into account as best as possible before comparing theoretical calculations with experiment.

Of course, a general statement such as the one beginning the foregoing paragraph cries out for an exception. It is well known (Bl 75) that, for nucleon and α-particle induced reactions, light particles are emitted from the compound system before equilibrium is attained. This pre-equilibrium emission is identified as a departure from the predictions for equilibrium decay. In particular, an excess number of particles appears with higher-than-average kinetic energies. Evidence for such pre-equilibrium emission (from the compound system) in heavy-ion induced reactions is scant and probably reflects the fact that the excitation energy is more easily spread over a larger number of nucleons in a heavy ion reaction. A possible exception is illustrated in Fig. 16 (Sa 77). The top row of the figure shows the probability of emitting x neutrons depending on whether the same compound nucleus is formed in the reactions ^{20}Ne + ^{150}Nd or ^{12}C + ^{158}Gd. Below is shown the average number γ-rays <M> emitted as a function of x. The ^{20}Ne results are consistent with statistical expectations. Assuming that the neutrons have a statistical distribution of energies, then the average number of γ-rays should increase as fewer neutrons are emitted. This behavior is also observed for ^{12}C + ^{158}Gd at lower bombarding energies. At an excitation

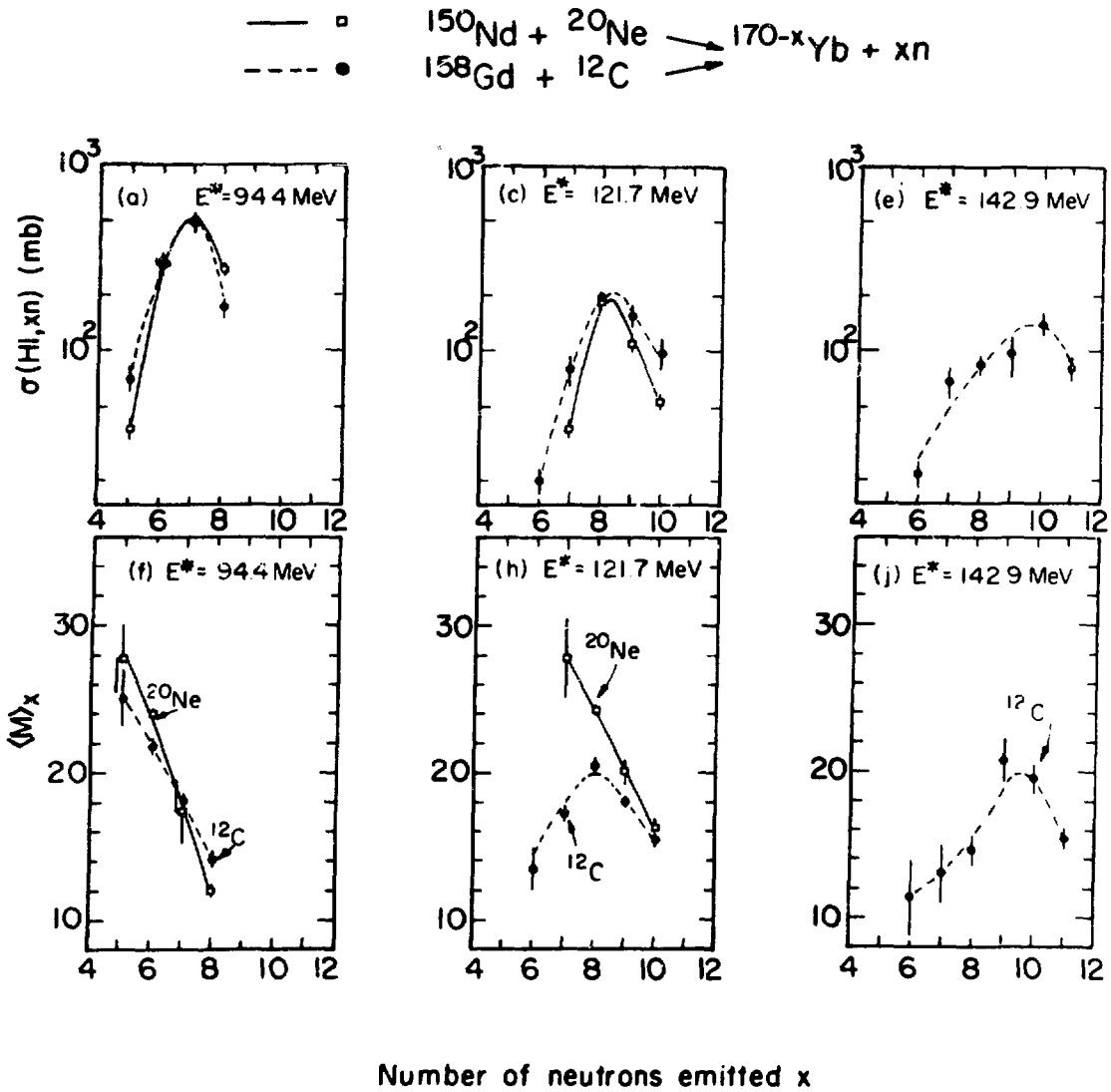

FIG. 16. Heavy-ion xn cross sections and γ-ray multiplicities for the reactions ^{12}C + ^{158}Gd and ^{20}Ne + ^{150}Nd (Sa 77). The decrease in $\langle M \rangle_x$ for small values of x observed for high energy ^{12}C bombardment suggests pre-equilibrium emission of neutrons.

energy of 121.7 MeV, however, one observes that $\langle M \rangle_x$ decreases with decreasing x. Part of this effect may arise from the opening of αxn channels which compete with the 7n and 6n channels, lowering the average compound nucleus angular momentum associated with these decays. However, it seems likely that the neutrons associated with the 6n and 7n decays now have a higher average kinetic energy (and most likely carry off more angular momentum). A plausible explanation for this is that the first neutron emitted had an anomalously large energy and therefore was emitted before equilibrium was attained. This could be verified by measuring the neutron spectra in coincidence with the residues. The cross section associated with this effect is of the order of 100 mb/sr.

The observation and further study of pre-equilibrium phenomena in heavy ion reactions is important in that it probes the early stages of compound nucleus formation. It is not clear how successful in these cases will be the theories developed for nucleon induced reactions, nor is it clear what are the best approximations to be made in treating the heavy-ion case. (The experimental results for ^{4}He projectiles and ^{12}C projectiles at the same MeV/nucleon are different.) The study, both experimental and theoretical, of pre-equilibrium emission in heavy ion reactions is thus at an early stage and should prove an exciting area in the future as the region of bombarding energy between 20 and 200 MeV/nucleon becomes accessible.

III. DEEP INELASTIC SCATTERING

Since the phenomenon of deep inelastic scattering began to attract attention in the early 1970's, an extremely large amount of experimental and theoretical work has been done. The basic features of the process have been established and the dependence of these features on the bombarding energy and charges of projectile and target has been mapped. The subject has been reviewed at the Caen Conference (Ga 76, Mo 76) and recently by Schröder and Huizenga (Sc 77b).

Most of the information gained so far in deep inelastic scattering is based on measurements of the energy, angle, and charge (or mass) of one of the fragments. These "first generation" experiments have been extremely productive. In the last year or two experiments have become more complex as more detailed questions are asked about the reaction mechanism. I want to select two aspects of the reaction mechanism and present, briefly, a number of recent experiments which focus on them. First we will consider the (spin) alignment of the fragments after collision and the amount of angular momentum transfer. The second aspect deals with the time scale of the collision and the mechanisms by which the damped energy is ultimately dissipated. The first topic is of relevance to theory insofar as the transfer of angular momentum is induced by nonconservative forces, i.e. by friction or viscosity, and this is of very current interest. The second aspect relates to the degree of equilibration of the rotating

di-nuclear complex (RDC) as we like to call the projectile-target system up to the point of scission. Simple and graphic questions are: Does the RDC emit particles before it scissions? Are there local hot spots (e.g. at the walls or in the neck) or does the system achieve a uniform temperature?

We ask what experiment can tell us.

A. Alignment and Angular Momentum Transfer

1) Particle experiments

In a simple classical picture of the deep inelastic reaction in which a portion of the angular momentum of relative motion is transferred to intrinsic degrees of freedom, the two fragments produced in the collision should have their angular momenta aligned perpendicular to the reaction plane defined by the beam and one of the fragments. The particles emitted by an excited fragment should exhibit an angular correlation which is indicative of this alignment. In particular, particles should be preferentially emitted in the reaction plane if the nucleus is aligned perpendicular to this plane. The situation is illustrated schematically in Figs. 17a and 17b. In Fig. 17a we

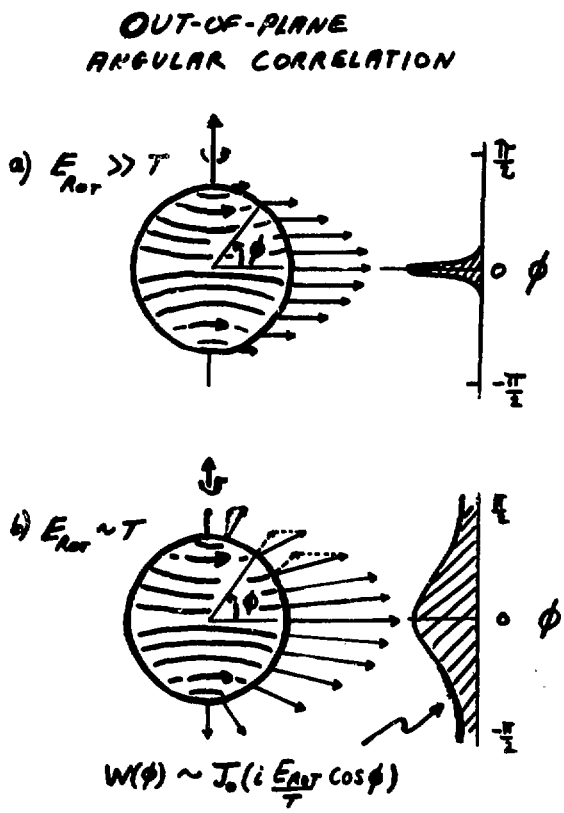

FIG. 17. (a) Particles released from the surface of a rotating sphere, all move in the equatorial plane provided their rotational velocity greatly exceeds the average radial velocity associated with their temperature. The angle of emission with respect to the equatorial plane is denoted by ϕ. (b) When the temperature and rotational energy are comparable, the out-of-plane correlation is broadened. The dashed arrows denote the components of the velocity due to temperature and the centrifugal force. The correlation function is given by Ericson and Strutinsky (Er 58).

consider a cold, rotating nucleus. The centrifugal force on any particle is parallel to the equatorial plan of the rotating nucleus which also lies in the reaction plane. If the nucleus has a temperature T, the emitted particles will have a radial velocity component which will smear out the sharp correlation of Fig. 17a and produce a correlation like that shown in Fig. 17b. Ericson and Strutinsky have derived the indicated expression for the angular correlation (Er 58). The quantity determining the anisotropy is the ratio of the emitted particles rotational energy to the temperature of the compound nucleus.

An experiment to measure the angular correlation and intensity of alpha particles in coincidence with the projectile-like fragment has been made by Ho et al. (Ho 77), for the reaction $^{58}Ni + ^{16}O$ (96 MeV). The experimental configuration is illustrated schematically in Fig. 18. The heavy-ion detector was at an angle of 35° with respect to the beam. The out-of-plane correlation was measured by moving the α-particle detector in a plane which cuts the reaction plane at angles of $\theta_\alpha = 35°$ for $\phi_\alpha = 0°$, and $\theta_\alpha = -145°$ for $\phi_\alpha = 180°$. The results are shown in Fig. 19 for α-particles in coincidence with carbon ions (solid points) and oxygen ions (open circles). (The data have been converted to the rest frame of the heavy fragment.) There is a clear out-of-plane correlation. The correlation is not symmetric about $\phi_\alpha = 90°$, however, as would be expected for equilibrium decay; we shall return to this point in Section IIIB. An analysis of the portion of the correlation from $\phi_\alpha = 90°$ to $\phi_\alpha = 180°$ yields a ratio of rotational energy to temperature which implies a spin J of 13 ħ for a temperature T = 2 MeV. (Complete alignment of J perpendicular to the reaction plane is assumed in deriving a value of J.) This value for the temperature is consistent with statistical model predictions and the shapes of the α-spectra (for $\phi_\alpha > 90°$). The value of 13 ħ agrees with results obtained from the measured γ-ray multiplicity (Al 75). Regardless of the precision with which the transferred angular momentum can be deduced by this procedure, the results shown in Fig. 19 demonstrate that the spin of the heavy fragment produced in this deep inelastic collision is aligned.

Light-particle emission is not the only possible mode of decay. In systems much heavier than mass 60, fission is an important de-excitation mechanism, and has the advantage of a well-developed theory of angular correlation and of previous experimental study (Va 73). This has been exploited in a recent experiment by Dyer et al. (Dy 77) in which a ^{209}Bi target was bombarded by 610 MeV ^{86}Kr ions. The experimental arrangement is shown schematically in Fig. 20. The angular correlation of one of the fission fragments in coincidence with the projectile-like fragment was measured both in plane and out of plane. Classical arguments similar to those applied in the previous example tell us that the fission fragments should be most intense in the reaction plane provided that the target-like fragment has a large angular momentum perpendicular to the reaction plane before scission.

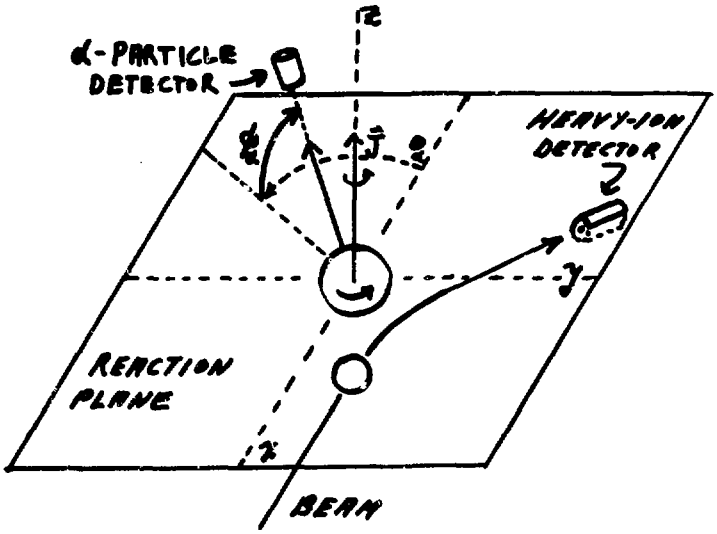

FIG. 18. Schematic representation of the experimental arrangement used to measure the correlation between α-particles and projectile-like fragment in the reaction $^{58}Ni + ^{16}O$ (96 MeV) (Ho 77). Note that ϕ_α is the polar angle between the emitted α-particle and the reaction plane.

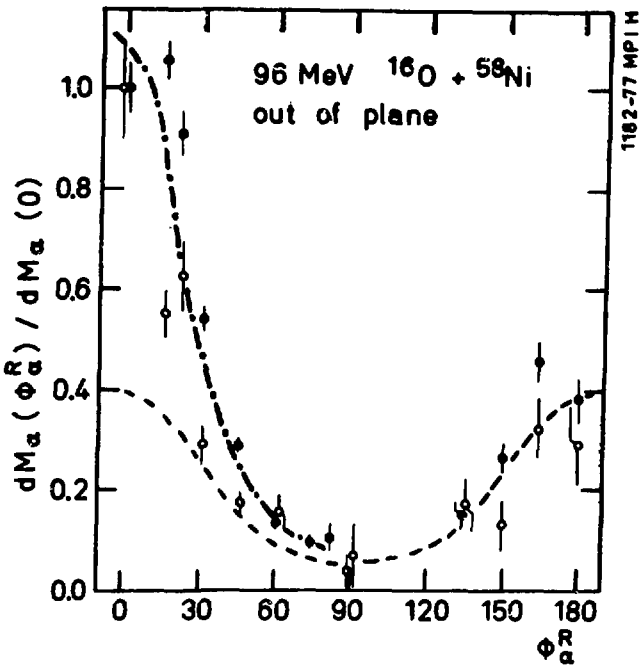

FIG. 19. The measured out-of-plane correlation. The angle ϕ_α^R corresponds to the angle ϕ in Fig. 18, but evaluated in the rest frame of the heavy fragment. The ordinate is the differential α-particle multiplicity (coincident α-particles per projectile-like fragment detected at 35°). The dashed lines are to guide the eye.

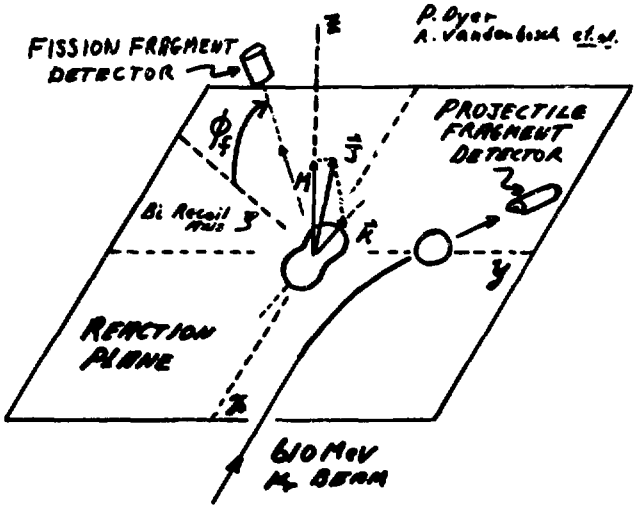

FIG. 20. Schematic diagram of the experimental arrangement used to measure the angular correlation of fission fragments in coincidence with the krypton-like fragment in the reaction $^{209}Bi + ^{86}Kr$ (610 MeV) (Dy 77).

The out-of-plane angular correlation for the fission fragments depends now on an additional quantum number K, the projection of the total angular momentum on the symmetry axis of the fissioning nucleus at scission. Thus we have

$$W^J_{MK}(\phi) \propto (2J + 1) \mid d^J_{MK}(\phi) \mid^2$$

and

$$\text{yield} \propto \sum_{JMK} P(J)\ P(M)\ P(K)\ W^J_{MK}(\phi)\ .$$

The distributions P(K), P(M) and P(J) represent the probabi' 'r finding the system with these quantum numbers and are obtain follows.

i) P(K): This is a property of the fissioning nucleus and

$$P(K) \propto \exp\left(-\frac{K^2}{2K_o^2}\right) .$$

K_o can be inferred from previous fission fragment angular correlation experiments.

ii) P(M): The alignment of the system is determined by the reaction mechanism. As a first estimate, complete alignment perpendicular to the reaction plane is assumed, M = J.

iii) P(J): The probability that the target-like fragment has total angular momentum J. The determination of this is the goal of the experiment. Assuming that the amount of angular momentum transferred, J, is proportional to the initial orbital angular momentum, ℓ, one has for deep inelastic collisions of Kr + Bi, $P(J) \propto 2J + 1$. This is because the partial cross section $\sigma_\ell^{D.I.} \propto 2\ell+1$. This distribution has an upper limit J_{max} which is the quantity to be determined by comparison with the data.

In Fig. 21 both the out-of-plane and in-plane angular correlations are shown. The in-plane counting rate is $\sim$ 25 times more intense than the rate perpendicular to the reaction plane. There is a slight in-plane correlation which should not be present if the system is completely aligned with M = J. An analysis has been made of both correlations allowing for less than complete alignment and other factors such as nonequatorial collisions and the existence of a lower limit (J_{min} = 18 ħ) on the angular momentum transferred in deep inelastic collision. The result is shown by the dotted lines and yields a value of J_{max} = 58 ħ. Dyer et al. are able to conclude that the maximum angular momentum transferred is between 50 and 70 ħ. J_{max} is estimated to be about 68 ħ in the limit that the Kr and Bi stick together and 39 ħ is the rolling limit. Thus the angular momentum transfer is larger than the rolling limit, less than (but consistent with) the sticking limit, and indicates that tangential friction is very important. A calculation of J_{max} has been made for this system by Gross et al. (Gr 75) and their prediction, J_{max} = 38 ħ, underestimates the transferred angular momentum. Agreement with experiment would presumably require increasing the tangential component of the friction. In any case, this experimental value for the transferred angular momentum represents an important datum for testing models for friction or viscosity in deep inelastic reactions. (The foregoing discussion is based on ref. Dy 77.)

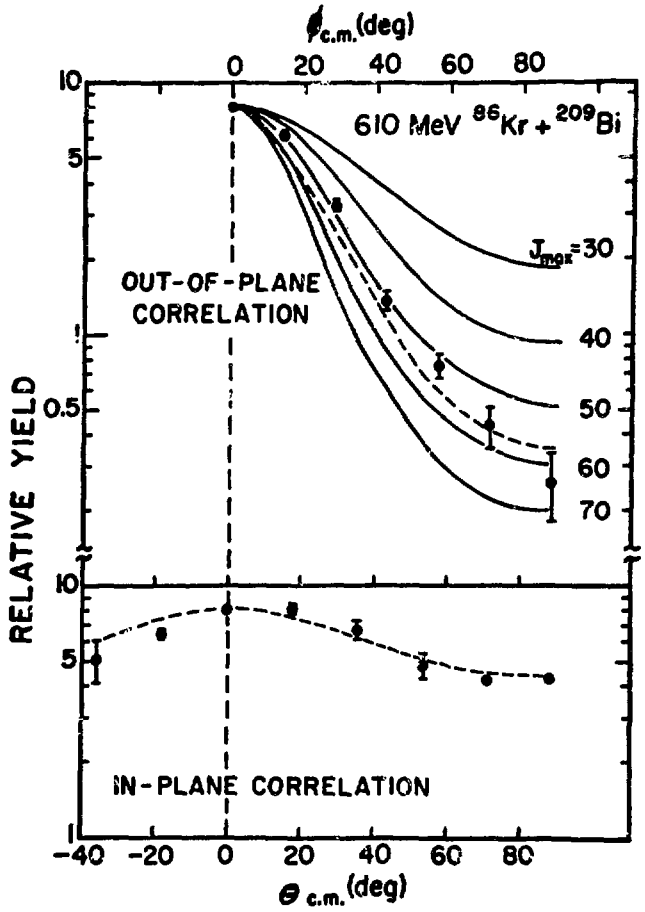

FIG. 21. The measured in-plane and out-of-plane correlation (Dy 77). Predictions of the out-of-plane correlation for various values of the maximum transferred angular momentum are shown. The dashed line is a simultaneous fit to both correlations which allows for some degree of non-alignment ($M \neq J$).

2) γ-ray experiments

After the excited fragments produced in the deep inelastic collision no longer have sufficient energy available for particle decay, γ-ray emission begins and completes the deexcitation process. The relative importance of γ-ray emission (in terms of the amount of excitation energy and angular momentum removed) varies with the mass and angular momentum of the excited fragment. In heavy nuclei where neutron emission is favored, γ-rays can carry away most of the angular momentum. Thus, the properties of the deep inelastic reaction products after scission can be reflected in the γ-ray emission. The problem, however, is how qualitatively to relate the experimental observations to the properties of the deep inelastic fragments before particle emission began.

Let us sidestep this problem for the moment, however, and first discuss two experiments which demonstrate that the residual nuclei can still be aligned when γ-ray emission commences. If the α-particle detector in the schematic diagram of Fig. 18 is replaced by a Ge-Li detector, the angular correlation for specific γ-ray transitions in the heavy fragment can be measured as a function of the species and energy of the light fragment. This has been done for the reaction $^{27}Al + {}^{16}O$ (100 MeV) by Van Bibber et al. (Va 77). Gamma-ray yields obtained in plane ($\phi_\gamma = 0$, solid data points) and out of plane ($\phi_\gamma = \frac{\pi}{2}$, open circles) are shown in Fig. 22. The γ-ray angular correlations expected for a nucleus aligned perpendicular to the reaction plane depend on the multipolarity of the radiation and are quite different for $\lambda = 1$ and $\lambda = 2$. Note in Fig. 22 that the yields of $\lambda = 2$ transitions $^{12}C(2^+ - 0^+)$ and $^{24}Mg(2^+ - 0^+)$ are largest for $\phi_\gamma = 0$ while the M1 transition $^{31}P(\frac{3}{2}^+ - \frac{1}{2}^+)$ is most intense perpendicular to the reaction plane. Although not all the E2 and M1 transitions in other nuclei observed in this work show the same pronounced anisotropy, these data are sufficient to demonstrate that some alignment exists. This experiment also shows that γ-ray angular correlations measured with a detector which records all γ-rays will in general be attenuated because E2 and M1 transition will be summed.

The second experiment to be mentioned shows not only that the fragments retain alignment but are also polarized in the direction perpendicular to the reaction plane. The goal of the experiment, by Trautman, de Boer et al. (Tr 77) was to measure the direction of rotation of the fragments for quasielastic and deep inelastic scattering and thereby test the negative-angle-scattering proposal of Wilczynski (Wi 73). γ-rays emitted in stretched transitions, regardless of multipolarity, will be circularly polarized in the direction of the angular momentum of the emitting nucleus. The amount of polarization varies as the cosine of the angle between the direction of the nuclear spin and the direction of the γ-ray. The direction of

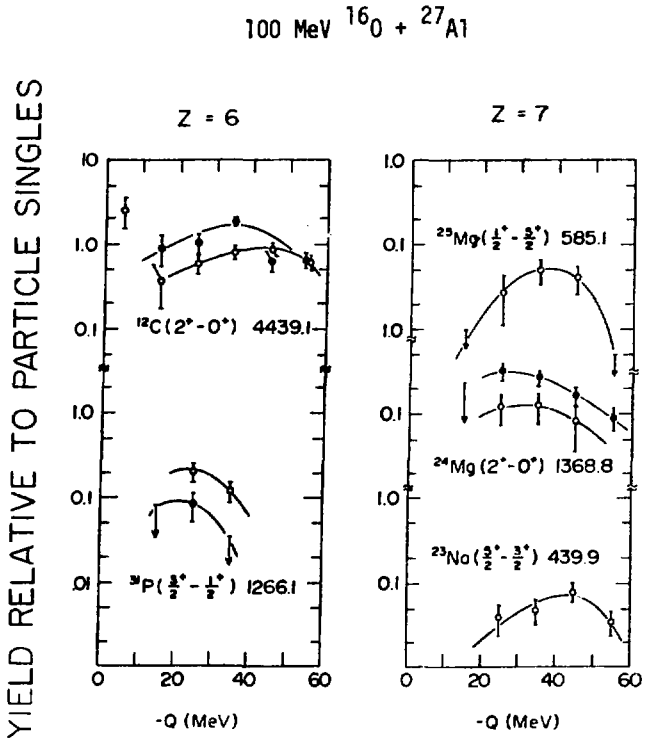

FIG. 22. The yield of specific γ-ray transitions in coincidence with Z = 6 and Z = 7 ions produced in the scattering of ^{16}O (100 MeV) by ^{27}Al (Va 77). The solid points represent the yield in the reaction plane, the open points perpendicular to the reaction plane. -Q is the energy lost in the collision.

the circular polarization can be measured by scattering the emitted γ-rays from the polarized electrons in magnetized iron. (The cross section for compton scattering at forward angles is larger if the electrons and γ rays are polarized in opposite directions.) Two polarimeters were employed in a symmetric configuration normal to the plane defined by two heavy ion counters at ± 35° with respect to the beam. (One reason for this is that the experimental effect to be measured is small, of the order of one percent, because only 2 out of the 26 electrons in an ion atom are polarized, and a very efficient system is needed.) The apparatus they used is sketched in Fig. 23. The reaction was Ag + ^{40}Ar (∿ 300 MeV) and was measured at GSI. They observed an asymmetry in the count rate which was of opposite sign for the quasielastic and deep inelastic components indicating that the fragments produced in the quasielastic and deep inelastic collisions spin in opposite directions. This confirms that deep inelastic scattering in this reaction is associated with a negative classical deflection angle. The degree of polarization was much larger for the quasielastic component than for the deep inelastic. This suggests that particle emission and other possible mechanisms we shall mention later contribute to a loss of polarization and alignment.

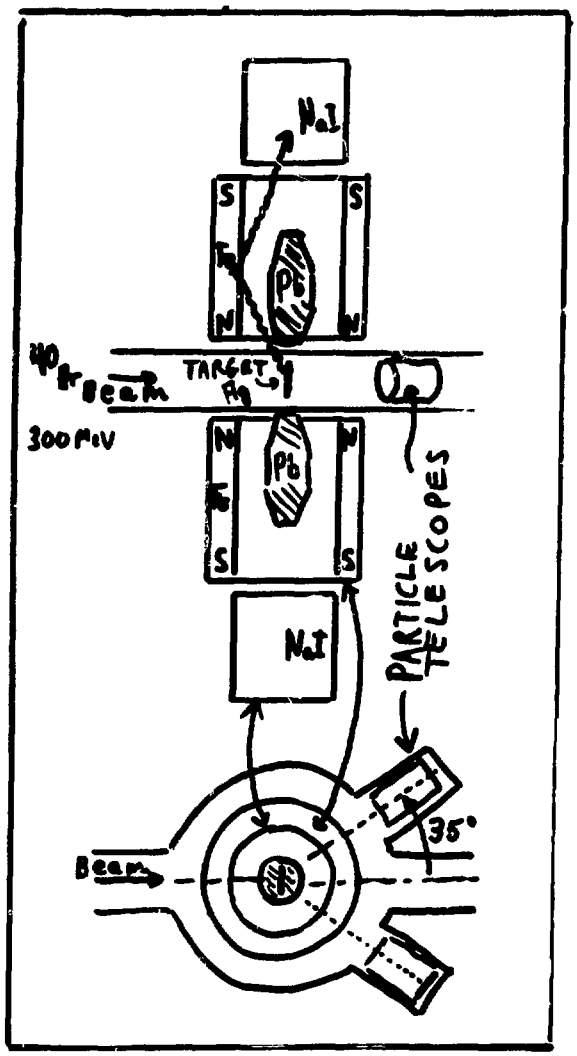

FIG. 23. Schematic diagram of the apparatus used by Trautmann, de Boer et al. (Tr 77) to measure the circular polarization of γ-rays emitted in quasi-elastic and deep inelastic reactions.

We return now to the question of relating γ-ray emission to the properties of the fragments before particle emission began.

The paths followed by the nuclei on the way to their ground states, and by the experimenter on the way back to the initial conditions, are illustrated in Fig. 24. The compound system is *the rotating dinuclear complex* which then separates into a heavy and a light fragment each having an average excitation energy and angular momentum. After particle emission ceases, an average number of γ-rays $\bar{M}_H$ and $\bar{M}_L$ are emitted by the heavy and light fragment, respectively. The sum of these two multiplicities is observed in coincidence with the light fragment as recorded by a counter telescope. The problem of working backwards from the observed average γ-ray multiplicity and average γ-ray energy to the quantities of interest involves estimating or measuring the effects of particle emission. Statistical model estimates can be made for very heavy nuclei which decay only by neutron emission. In lighter systems this procedure would seem less reliable and the empirical approach is preferred. One measures the multiplicities for evaporation residues in which the E^* and J (of Fig. 24) are known. A functional dependence of M_γ on E^* and J can

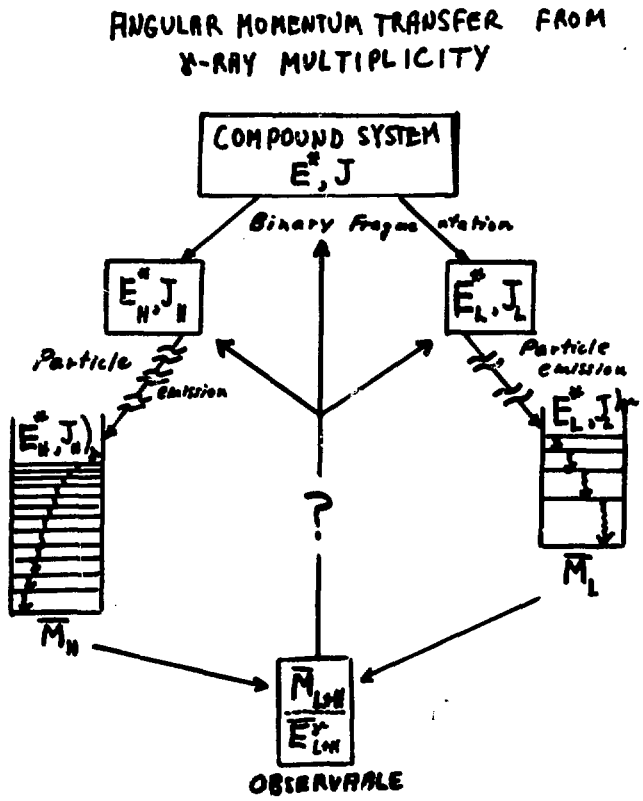

FIG. 24. Illustration of the various stages of decay in a deep inelastic reaction. In order to deduce the transferred angular momentum $J_L + J_H$ from the measured multiplicity $\bar{M} = \bar{M}_L + \bar{M}_H$, a correction for the amount of angular momentum removed by particle emission must be made.

thus be deduced. The crucial assumption is that the decay of the deep inelastic fragment follows the same rules as that of a compound nucleus.

Measurements of the average γ-ray multiplicity, $\bar{M}_\gamma$, have been made on a number of systems (Al 75, Ish 76, Bo 76, Gl 77, Pe 77, Da 77) (see Pe 77 for a recent review). The manner in which the various authors have estimated the effects of particle emission has varied, but the end results have generally yielded values of the angular momentum transfer in between those corresponding to rolling and sticking. Several examples are as follows.

The value of $\bar{M}_\gamma$ in the reaction $^{14}N + {}^{93}Nb$ at $E_{^{14}N} = 120$ MeV has been measured by Ishihara et al. (Ish 76). The results are shown in Fig. 25 for both the deep inelastic component and the quasielastic component as a function of the mass of the light product. The dashed line is a prediction of M_γ assuming the reaction partners reach a stage in which their surfaces stick together and the system undergoes rigid rotation before scissioning. The solid line pertains to quasielastic reactions in which the exchange of mass is assumed responsible for a transfer of angular momentum. In relating the transferred

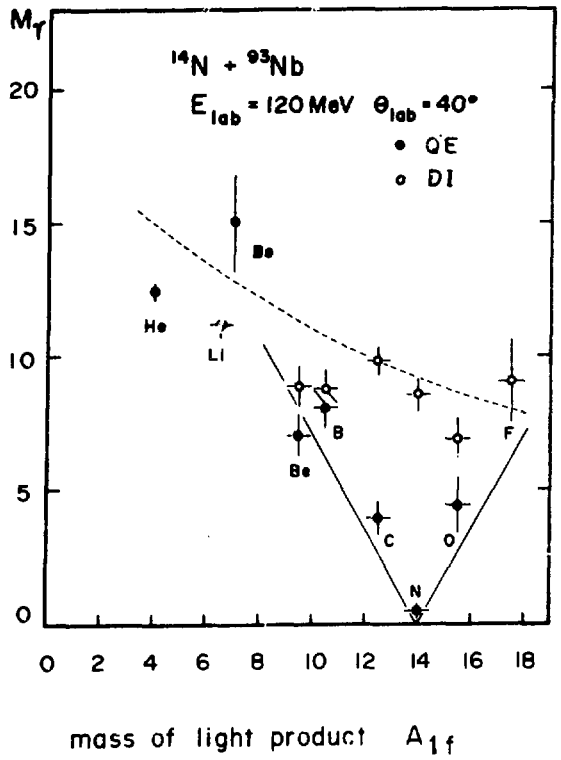

FIG. 25. Measured γ-ray multiplicity for the reaction $^{14}N + ^{93}Nb$ (Ish 76).

angular momentum J to the γ-ray multiplicity, the equation $J = 2.4\ M_\gamma$, was used. A portion of this amount, $J = 1.7\ M_\gamma$ represents the angular momentum associated with γ ray emission alone whereas the remainder $J = 0.7\ \tilde{M}_\gamma$ corresponds to the angular momentum carried off by particle emission. The latter was estimated with a statistical model.

Qualitatively similar results were obtained for a somewhat heavier system, Ag + ^{20}Ne (175 MeV) by Glässel et al. (Gl 77). Figure 26 shows the multiplicity measured as a function of the light-fragment atomic number for several scattering angles. The more damped the energy of a reaction product, the higher the multiplicity. M_γ increases in general for larger scattering angles suggesting that the compound system has lived longer and therefore had more time to approach a sticking limit. The agreement for smaller values of Z is better with a sticking limit obtained from a lower initial orbital angular momentum (50 ħ). This is interpreted as a consequence of the lower Z reaction products being preferentially produced by lower ℓ-waves. The relationship between M_γ and transferred angular momentum in this case is assumed to be $J = 2\ M_\gamma$, the argument being that γ-ray multipolarities less than 2 are offset by the neglect of the angular momenta carried off by neutrons. The results, again, lie in between the rolling and sticking limits.

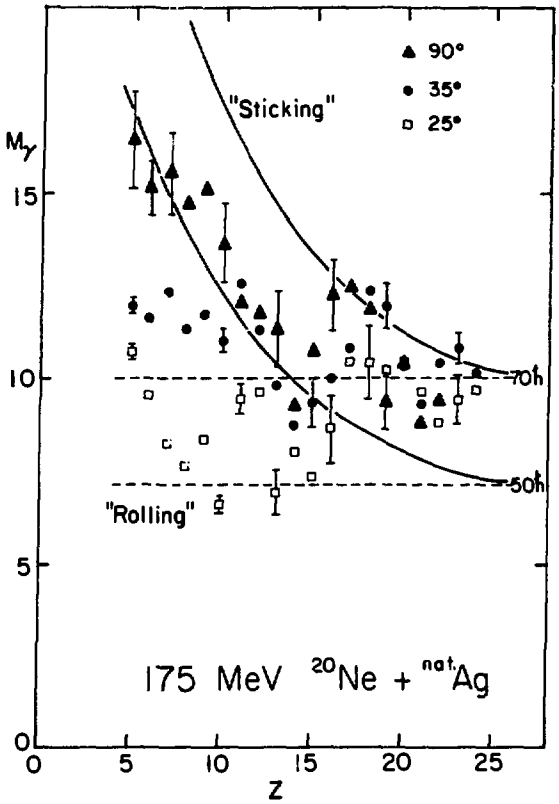

FIG. 26. Measured values of M_γ for the deep inelastic products produced at angles of 90°, 35° and 25° in the reaction Ag + ^{20}Ne (175 MeV) (Gl 77).

The results for a much heavier system, Au + Cu (443 MeV) are shown in Figs. 27 and 28 (Be 76b, Pe 77). The value of M_γ as a function of the energy of particles detected at 49° is given in Fig. 27. The multiplicity increases as a function of energy loss through the range of events corresponding to partial and complete damping. In Fig. 28 the value of M_γ measured at two angles is plotted versus mass asymmetry and compared with various sticking model predictions assuming $J = 2\ M_\gamma$. The prediction includes the effect of deformation at the scission point. The initial orbital angular momentum $\ell_i = 124$ is near the weighted average of angular momenta over the range $\ell_i = 0$ (assuming no fusion) to $\ell_i = 175$ (the maximum ℓ-value contributing to the deep inelastic collision. The value $\ell_i = 175/2$ is shown for additional reference.

In the reaction ^{58}Ni + ^{40}Ar (280 MeV), the measured multiplicities are below the rolling limit if $J = 2\ M_\gamma$ and no correction for particle emission is made (Bo 76). These authors have also measured the α-particle multiplicity and suggest that the amount of angular momentum removed by particle emission together with a more realistic calculation of the transferred angular momentum (i.e. one including deformation) would bring theory and experiment much closer together.

While most of our information on angular momentum transfer has come from coincidence experiments observing the decay products of

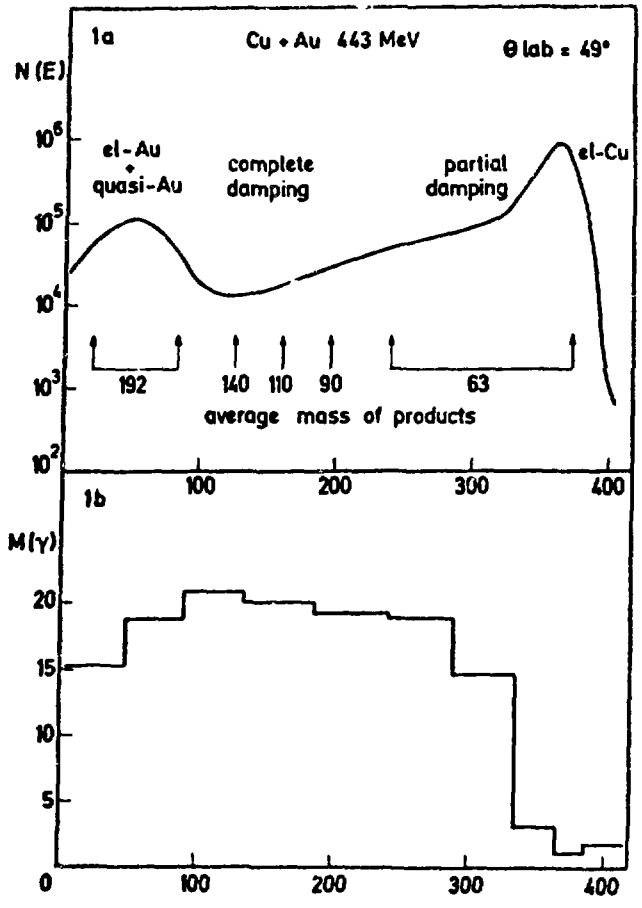

FIG. 27. Measured values of M_γ for deep inelastic products produced in the reaction Au + Cu (443 MeV) (Be 76b, Pe 77).

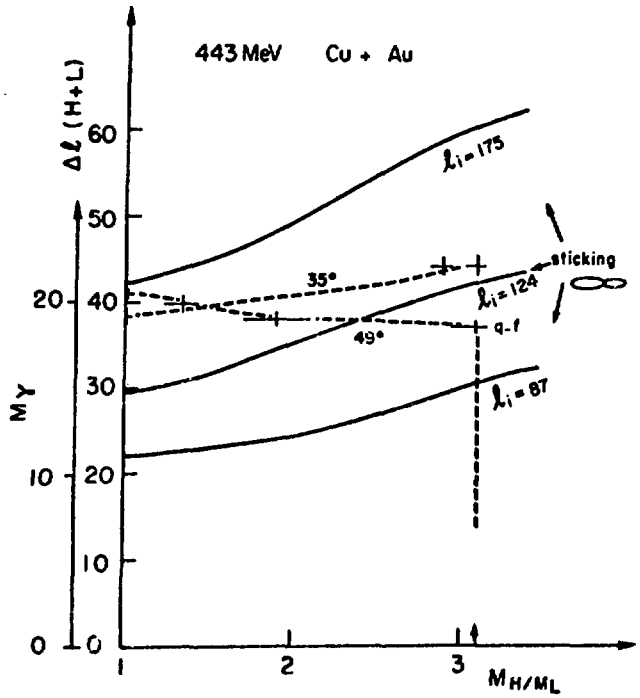

FIG 28. The multiplicity of the deep inelastic products as a function of the masses of the reaction products (Be 76b, Pe 77). Predictions of the sticking model for various initial orbital angular momenta are shown.

the primary fragments, it should be noted that there is one experiment in which angular momentum transfer has been deduced from the measurement of the total kinetic energies of the primary fragments as a function of bombarding energy. This has been done by Braun-Munzinger et al. (Br 76, Co 77b). The analysis assumes that the Coulomb separation energy is independent of bombarding energy and that the amount of transferred angular momentum (which reduces the rotational portion of the total kinetic energy) is proportional to the initial orbital angular momentum. The deduced constant of proportionality agrees well with the sticking model.

The measurements of the average γ-ray multiplicity described above are valuable in that they provide (albeit with accompanying assumptions and uncertainties) a measure of the amount of angular momentum transfer. Measurements of the angular correlation of the γ-rays, averaged over all γ-ray energies, in principle give information on the degree of alignment, but it is here that things begin to be more complicated than the foregoing descriptions of the experiments and their interpretations would suggest. Measurements of the out-of-plane γ-ray angular correlation averaged over all γ-ray energies) for the reactions ^{14}N + ^{93}Nb (Ish 76), Ar + Ni (Bo 76), and Cu + Au (Pe 77) indicate a rather small anisotropy, i.e. the out-of-plane count rate is generally ∿ 80-90% of the in-plane count rate. Perrin

and Peter (Pe 77) suggest (particularly for the heavy system Cu + Au) that this lack of alignment may arise from sources other than M1-E2 mixed multipolarity or misalignment caused by particle emission. Making the analogy with fission, the fragments at scission can, through bending, wriggling, or twisting modes of motion (Ni 65), induce angular momenta in the primary fragments which are not in the plane of the reaction defined by the beam and one of the fragments. For the first two modes of motion, the induced angular momentum would be perpendicular to the direction of the separating fragments; in the third case, it would parallel this direction. Measurements of angular correlations of discrete γ-rays in the spontaneous fission of ^{252}Cf by Wolf and Cheifitz (Wo 76) suggest that twisting is not an important mode of motion and that bending and/or wriggling dominate. The results of Dyer et al. (Dy 77), (Fig. 21) should enable an upper limit to be placed on these bending and wriggling contributions and it would be very interesting to see what a quantitative analysis would yield. However the induction of additional angular momenta in the fragments through dynamical processes at scission does not imply that current analyses of γ-ray multiplicity experiments overestimate the amount of angular momentum transferred through friction in the portion of the reaction leading up to scission. This is because the average angular momentum (i.e. the first moment of the distribution) obtained after averaging the vector sum of the aligned component and the induced component over all directions of the induced angular momentum would not be much different than that due to the aligned component alone. The second moment, or width, of the angular momentum distribution would be very different, however. This brings us to the consideration of higher moments of the multiplicity distribution.

Just as the average number of γ-rays reflects an average angular momentum, the distribution of the number of γ-rays about the average reflects a distribution in angular momenta. Knowledge of the distribution of angular momenta in the reaction products is very desirable. Higher moments of the multiplicity have been reported for compound nucleus decay (Ha 75, Sa 76) and used to deduce spin distributions.

In the case of deep inelastic collisions, the second and third moments of the γ-ray multiplicity have been measured by Dayras et al. (Da 77) for the reaction ^{63}Cu + ^{20}Ne (164 MeV). Data were also obtained for the evaporation residues produced in the reaction ^{63}Cu + ^{12}C (130 MeV). The results are shown in Fig. 29. The moments of the γ-ray multiplicity are in each case evaluated at a single scattering angle and over a narrow energy window at the peak intensity of the deep inelastic yield for each atomic number. (In this portion of the spectrum, the contribution from reactions induced on carbon and oxygen contaminants in the target is small). One would expect that the width of the multiplicity distribution would be less in the case of the deep inelastic collision; the argument is as follows. The evaporation residues contain angular momenta from 0 to ℓ_{crit} and, for a $(2\ell+1)$ triangular

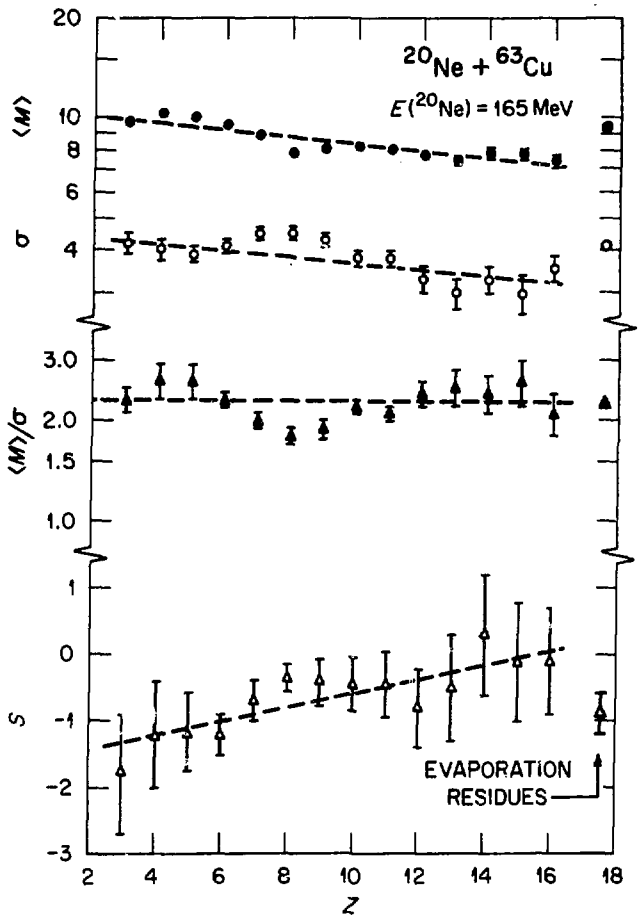

FIG. 29. The multiplicity M, width σ, and skewness S measured for the deep inelastic scattering of ^{63}Cu + ^{20}Ne (164 MeV), (Da 77). The straight lines are to guide the eye. The projectile-like fragments with atomic number Z were detected at 20° lab. M, σ, and S are evaluated for those particles having energies at the peak of the deep inelastic yield. The trend of M to decrease with Z is in agreement with the sticking model. Also shown are the results for evaporation residues produced in the fusion of ^{63}Cu + ^{12}C (130 MeV). Note that the limit of M, σ, and S as Z decreases approaches that of compound nucleus decay. The quantities M, S and σ are defined in ref. Sa 76.

distribution, we would expect $\frac{\langle M \rangle}{\langle \sigma \rangle} \simeq \sqrt{8} \simeq 2.8$. We observe a value of 2.3 and attribute the discrepancy to additional broadening arising from particle emission and statistical cascades. In the case of deep inelastic scattering we would expect a narrower distribution of angular momenta varying from $f \times \ell_{crit}$ to $f \times \ell_{gr}$ where f represents the fraction of angular momentum transferred. Indeed, this should represent an upper limit on the width since we have selected a narrow angular and energy region of deep inelastic products and, if anything, this would narrow the range of impact parameter. Neglecting broadening from particle emission and from other effects such as statistical cascades, a variance $\sigma^2 \approx 0.6$ would be expected for the multiplicity distribution. Assuming the broadening of the distribution by the effects mentioned above can be derived from the value deduced from the evaporation residues, a variance of $\sigma^2 \simeq 7.6$ is predicted. Yet this value is only about one half of the measured variance. For example, $\sigma^2_{experimental} = 15$ for deep inelastic products with Z = 5. This implies an additional broadening of the transferred angular momentum distribution. Possible explanations for this are as follows.

i) The distribution of initial angular momenta contributing to deep inelastic scattering is much broader than $\ell_{crit} \rightarrow \ell_{gr}$. Even if this were the case, however, the selection of reaction products at a given energy and scattering angle should correspond to a narrow population of initial angular momenta. This follows provided that the angular momentum transfer J is proportional to the initial orbital angular momentum, $J = f \times \ell$.

ii) The constant f in the relation $J = f \times \ell_i$ is not a constant but has itself a distribution. This would imply statistical processes in the transfer of angular momentum, a proposition which does not seem unreasonable.

iii) There are additional angular momenta induced at scission (the bending and wriggling just discussed) which would certainly broaden the angular momentum distribution while not greatly affecting the average value. This possibility has been suggested by Perrin and Peter (Pr 77).

iv) We have assumed that the excited fragments produced in the deep inelastic collision reach equilibrium and decay in the same manner as compound nuclei produced in fusion reactions. This assumption may not be valid.

The last item introduces another (and our last) topic. What in fact are the modes of decay by which the deep inelastic complex and its fragments rid themselves of excess energy and angular momentum?

B. Time Scale and Mechanisms for Decay

The length of time for which the system produced in a heavy-ion collision holds together is a basic parameter. Although it cannot be measured directly, (at least not for the short time scales of deep inelastic collisions) it can be inferred from analyses of the reaction products and orbit calculations (see, e.g. Bo 75) and from correlations of energy loss and mass transfer (Hu 76). However, rough estimates of the time scale can be made using very simple arguments.

Considering the rotational motion, we have an angular velocity ω, and an angle of rotation θ through which the fragments remain in contact.

$$\tau_{DI} = \theta/\omega$$

We can estimate a rotational energy, an orbital angular momentum ℓ, and a moment of inertia, $\mathcal{J}$ and use

$$\omega = 2E_{ROT}/\hbar\ell$$

or

$$\omega = \hbar\ell/\mathcal{J}$$

to obtain ω. For example, we could take $\ell \approx \frac{5}{7}\ell_{gr}$ corresponding to rolling fragments and $E_{ROT} = E_{c.m.} - E_{coul} + Q$. A typical angle θ would be ~ 1 radian for a forward peaked reaction.

Considering the radial motion, the time for the fragments to move together and apart is governed by the Coulomb force f and the radial velocity, v_{rad} (Mo 76)

$$\tau_{DI} = \frac{2\mu\, v_{rad}}{f_{coul}} = \frac{\sqrt{2}\ \hbar\ell}{E_{coul}} .$$

Most of the reactions studied experimentally thus far have collision times in the range of 4-20 (10^{-22} sec).

We can also make estimates of the time it takes an equilibrated excited nucleus to emit a particle (proton, neutron or α-particle). An empirical fit to measured widths of compound nuclei in the mass range A = 20 - 100 yields (St 74)

$$\Gamma\ (\text{MeV}) = 14 \exp\left(-4.69\sqrt{A/E^*}\right)$$

where E^* is the excitation energy of a nucleus with mass A. Relating the temperature T to the excitation energy as $E^* = aT^2$ where a = A/7.5,

we have

$$\tau_{part} \simeq 0.5 \exp (13/T)$$

where T is in MeV and τ_{part} is in units of 10^{-22} sec. An excitation energy of 1.2 MeV/A yields a temperature of 3 MeV and a lifetime $\sim 40 \times 10^{-22}$ MeV sec.

Figure 30 relates ω, τ, E^*/A and T for an angular rotation of 1 radian. We see from this figure that if local temperatures of $\sim$ 3-5 MeV, i.e. excitation energies of $\sim$ 1 - 4 MeV per nucleon should be produced in a deep inelastic collision, then the lifetime for particle emission will be sufficiently short that the complex will eject light particles before it scissions. We say local temperatures because total center-of-mass bombarding energies in most experiments are less than $\sim$ 7 MeV/$A_{projectile}$ and therefore the achievement of, say, 3 MeV/A nucleon in some region requires a pronounced concentration of energy, i.e. what might be called a "hot spot".

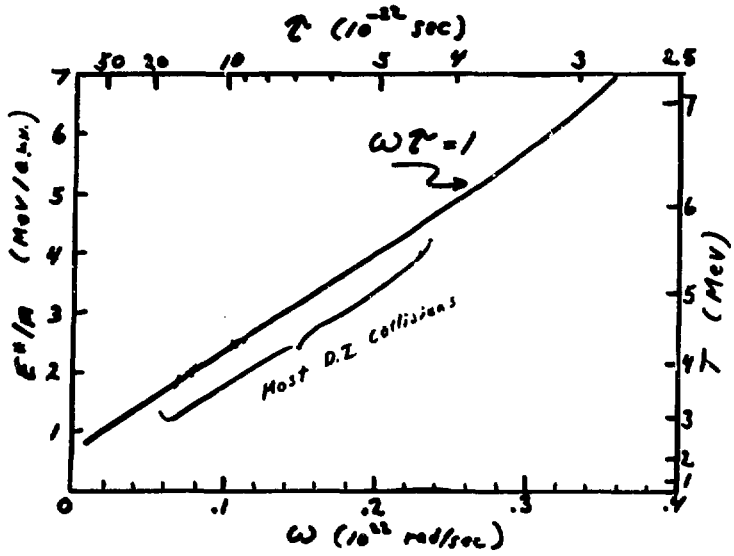

FIG. 30. Relationship of the excitation energy/nucleon and equivalent temperature to the lifetime τ against particle decay of a system in statistical equilibrium. ω is the angular velocity of the rotating dinuclear system. Given either abscissa (τ or ω), either of the ordinates then yields the temperature or excitation energy/amu for which the lifetime against statistical particle emission is equal to the lifetime τ of the dinuclear complex or to the time it takes the system to rotate one radian. Most deep inelastic collisions studied to date have lifetimes in the region indicated.

Experimental evidence for such phenomena would consist of a departure of observed yields (energy distributions, angular distributions) from what would be expected if equilibrium had been attained.

In the experiment by Ho et al. (see Figs. 18, 19) a departure from equilibrium manifests itself by an excess yield of α-particles at forward angles. This appears in the out-of-plane correlation shown in Fig. 19 and also in Fig. 31, which presents the yield of α-particles in the reaction plane. There is a strong peaking of the yield at forward angles, in contrast to the isotropic angular distribution which would have been expected in the classical picture of emission from a completely equilibrated and aligned rotating nucleus. Using the simple expression we have just given ($\omega = \hbar\ell/\mathcal{J}$) and $\theta = 2\sigma_\theta$ where σ_θ is the experimental standard deviation of the angular distribution in Fig. 31. The result is $\tau_\alpha \lesssim 20 \times 10^{-22}$ sec independent of whether it is the deep inelastic complex with 33 units of angular momentum (before scission) which emits the α-particle or an excited ^{58}Ni fragment with 12 units of (transferred) angular momentum. In Fig. 30 we see that such a lifetime corresponds to a local temperature of $\gtrsim$ 3.3 MeV. A statistical analysis of the α-particle energy spectra (intensity $\propto$ exp(- E_α/T) yields temperatures of 3-4 MeV for the α-particles emitted

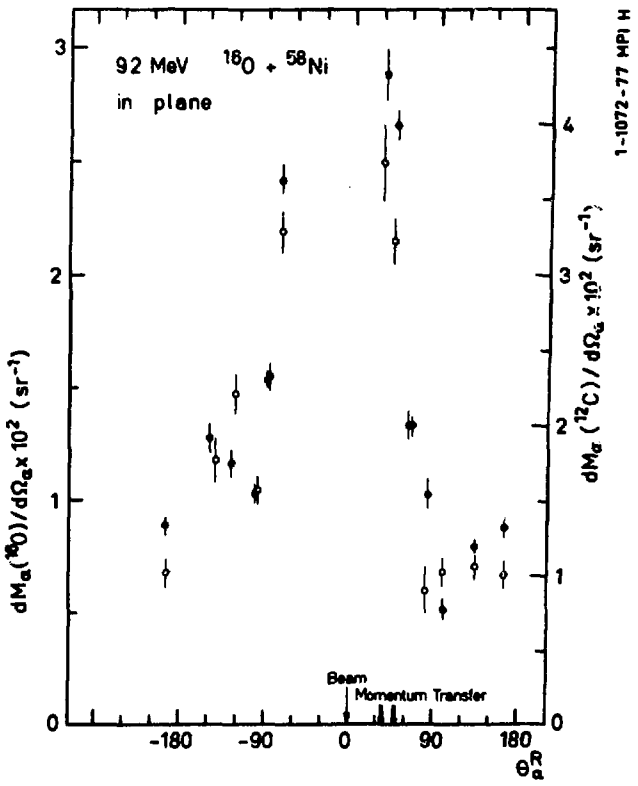

FIG. 31. The in-plane angular correlation of α-particles in coincidence with carbon ions (solid points) or oxygen ions (open circles) detected at -35° lab (Ho 77). The angle with respect to the beam is measured in the frame of the heavy residual nucleus. The strong forward peaking is not consistent with an isotropic decay of an equilibrated residual nucleus.

in the forward hemisphere and a temperature, as we have already noted, of 2 MeV for particles emitted in the back hemisphere. Thus, these features of the reaction (angular distributions and shapes of energy spectra) suggest emission of α-particles either before scission of the deep inelastic system or immediately thereafter and before the heavy fragment had time to equilibrate. Note that the fraction of the alpha particle yield corresponding to preequilibrium emission is ∿ 50%. However, this does not represent a major fraction of the total decay since the α particle multiplicity itself is only ∿ 10% (for detected O) and ∿ 20% (for detected C).

A kinematic analysis of the most probable α-particle energy indicates that this energy is independent of angle if it is calculated in the rest frame of the heavy fragment. Provided that this would not also be the case if the rest frame of the dinuclear complex (i.e. ^{16}O + ^{58}Ni) were used instead, this suggests that the α-particles are emitted after scission. (This analysis also rules out projectile breakup as an important mechanism.) To explain these features, Ho et al. propose the formation of a local hot spot with a temperature of T ≈ 3.5 MeV, and an area covering ∿ 20% of the sphere to explain the observed angular correlation, energy spectra and α-particle multiplicities.

Mechanisms for the production of preequilibrium α-particles have been discussed recently by Gross and Wilcyznski (Gr 77). In their model, a strong radial friction induces α-particle emission on the opposite side of the nucleus from where projectile and target first come into contact. Such a picture could be consistent with the data of Ho et al.

Other experiments of this type have been reported by Harris et al. (Ha 77), ^{27}Al + ^{16}O (65 MeV), and Ishihara et al. (Ish 76b) ^{93}Nb + ^{14}N (95 MeV). They all have in common the fact that anisotropic in-plane correlations between the emitted light particle (p or α) and the light fragment are observed.

The emission of light charged particles in a deep inelastic collision involving much heavier nuclei is being studied by a group at the SuperHilac (Al 77). Krypton-like products are detected at a forward angle of 36° or 42° and light charged particles are observed with a counter telescope at angles varying from 81° to 315° in the reaction plane. The approach is to use the knowledge (including empirical systematics) of compound nucleus decay to identify that portion of the α-particle yield consistent with decay of equilibrated Kr and Au fragments. The purpose of the experiment, then, is to determine the amount, if any, and properties of charged particle emission which might correspond to preequilibrium emission.

The velocity-vector diagram of Fig. 32 shows how the kinematics of the reaction is used to identify the evaporation products. The

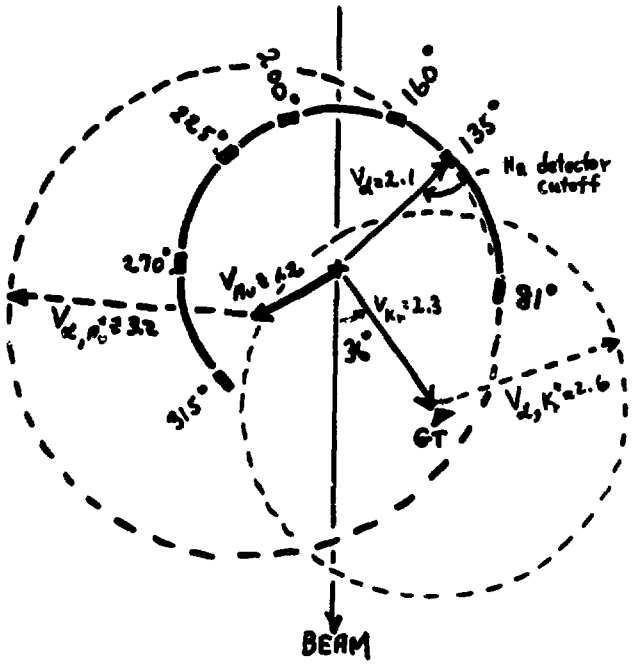

FIG. 32. Velocity vector diagram illustrating the kinematics for statistical α-particle emission in the reaction Au + ^{86}Kr (724 MeV) (Al 77). The scattered Kr ion is detected at 36° by a gas telescope (GT) and has an average velocity of 2.3 cm/ns. An alpha particle evaporated from the Kr would have a velocity of 2.6 cm/ns. Only the solid state telescope positioned at 81° could therefore detect α-particles evaporated from Kr. A similar kinematic circle for the α-particle evaporated from the Au fragment is also shown.

threshold for detection of an α-particle in this experiment is ∿ 9 MeV or ∿ 2.1 cm/ns. The average velocity of an evaporated α particle is the sum of its velocity relative to the Kr or Au which emitted it and the velocity of the Kr or Au. Because of the higher Coulomb barrier, α-particles evaporated from the Au-like fragment can be well above the threshold in the detectors located at 200°-315°. α-particles evaporated from the Kr will only be observed in the detector at 81°.

The following results are preliminary. The α-spectra observed at 225° and 270°, when transformed to the frame of the Au fragment, are just what one expects for evaporation of α's from an excited but equilibrated Au-like nucleus. This evaporation portion is subtracted bin by bin from the spectra at other angles. The α-spectra at 81°, when transformed to the Kr frame, is entirely consistent with α-evaporation from a Kr-like fragment. This evaporation spectrum is then subtracted from the spectra at other angles. (The subtraction is done in individual energy bins because of the 9 MeV threshold.) At angles other than 81°, 225°, and 270° there is a significant number of events left over after subtraction of the evaporation component. These α-particles have a higher average energy than that expected for evaporation from either of the fragments - in fact, this energy is ∿ 40 MeV, slightly above the Coulomb barrier for Z = 36 + 79 = 115. Figure 33 shows the measured energy-integrated yields above threshold in the various detectors before and after subtraction of the evaporation component vs. the average center-of-mass angle between the α-particle and the detected Kr fragment. The magnitude of the total yield at some angles is affected by the 9 MeV threshold. The preequilibrium yield is not strongly affected since the energies are higher. The preequilibrium α-particles are preferentially observed at angles near 90° and 270°, i.e. normal to the direction of motion of the Au and Kr fragments. This is illustrated schematically in Fig. 34 and is a situation similar to that encountered in fission where fast α particles appear to be ejected at scission at right angles to the neck focussed by the Coulomb force of the two fragments. In the present case, however, the α-particle energies are higher (Va 73). Although there is some evidence for the preequilibrium emission of protons in this experiment, (when the heavy-ion detector was at 42°) it does not seem to be as large a portion of the yield as is the case with the α-particles.

The experiments on ^{16}O + Ni and Kr + Au which we have just discussed indicate that the emission of light particles can occur on the same time scale as the deep inelastic collision. In both experiments there is evidence that this "preequilibrium" emission takes place at or immediately after the point at which the two fragments separate. (Preequilibrium decay does not happen exclusively, however. Many of the events correspond to the excited fragments reaching equilibrium before decay.) The preequilibrium particles are the means we have for studying the properties of nuclear systems under extreme conditions of temperature.

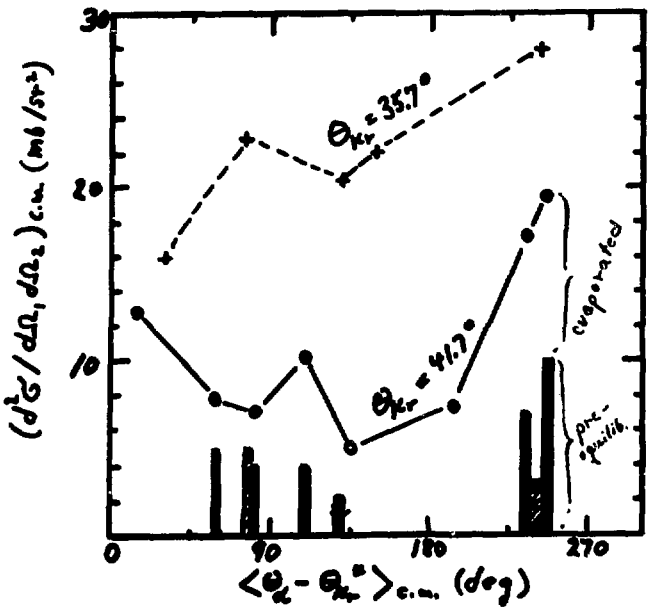

FIG. 33. Preliminary results of coincidence measurements (A1 77) with the gas telescope at 35.7° and at 41.7°. The circles and crosses represent the total number of α's above the detector threshold. The lines are only to guide the eye. The abscissa is the average center-of-mass angle between the emitted α and the Kr-like fragment. The vertical bars represent the α-particle yield remaining after the contribution due to evaporation from either fragment has been subtracted (solid bars, 41.7°; matched bars, 35.7°). There is a preference for α-particles to be emitted at nearly right angles to the direction of the Kr ion.

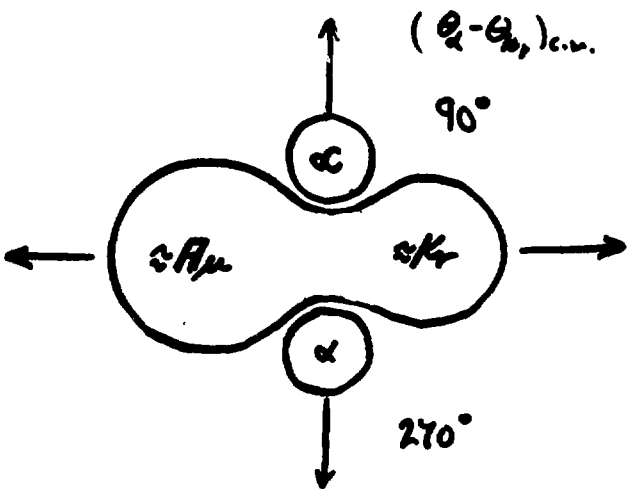

FIG. 34. Illustration of the emission of α-particle at right angles to the axis of symmetry at scission. The Coulomb forces of the two main fragments can "focus" the alpha particles to angles near 90°.

IV. SUMMARY AND CONCLUSIONS

We have just seen the results of a very large number of experiments. What are their distinguishing features, what do they tell us about heavy-ion collisions and how do they relate to nuclear theory?

A. Fusion

The process of fusion represents the most complex of heavy-ion collision processes in that the final state has all degrees of freedom excited in a statistical way. Phenomenologically, however, fusion has been the process most easily described with a small number of degrees of freedom and very few parameters. We wish to extend our knowledge of fusion beyond the stage of phenomenology and proceed further toward the final state. The initial stages of fusion as the two ions approach must involve low nuclear densities and therefore only a few nucleons. We ask whether the nature of the fusion process is such that the valence nucleons affect the outcome. Microscopic calculations suggest this might happen. Experiments on the fusion of light heavy ions at sub-Coulomb energies show in some cases pronounced changes in the energy dependence of σ_{fus}. These changes occur with variations of one or two units in the mass number of the colliding system (Figs. 5, 6). Microscopic calculations of the complex potential as well as of the real potential will probably be necessary to understand the changes in behavior from system to system.

Fusion cross sections measured at energies above the Coulomb barrier at the point where direct reactions become an important part of the reaction cross section also show large variations with mass number of the colliding system (Fig. 9). These variations, of the order of 200 mb, are much larger than variations in $A^{1/3}$. Until the measurement of σ_{fus} for $^{15}N + {}^{12}C$ there was an apparent systematic dependence of σ_{fus} on the shell closure at ^{16}O. These experimental data on fusion cross sections both above and below the Coulomb barrier provide an opportunity for testing microscopic theories of heavy-ion fusion.

In heavy-ion systems studied with projectiles of $A < 40$ the most important factor limiting fusion has been the dynamics of the entrance channel. These dynamical requirements for fusion have been condensed into a one dimensional prescription - penetration to a critical radius. By measuring σ_{fus} at a sufficiently high bombarding ($E_{^{14}N} \simeq 18$ MeV/A) it has been possible to observe a decrease in σ_{fus} indicating a limitation more restrictive than penetration to a critical radius (Fig. 10). The maximum angular momentum with which it has been possible to form ^{26}Al (Fig. 11) is consistent with value predicted by the rotating liquid drop model. Because the number of nucleons in a system as light as ^{26}Al, is relatively small, microscopic calculations are more manageable and economical. Differences between macroscopic and microscopic treatments can be explored in a system for which such differences are more likely, and for which there is an experimental result.

The distribution of residues of the compound system can be calculated rather well (Fig. 12). These calculations suggest that highly excited compound nuclei undergo rigid rotation for large angular momenta and are deformed. This is consistent with measurements of the critical angular momentum as a function of excitation energy. Statistical calculations are of value in identifying non-compound processes such as preequilibrium decay (Fig. 16) and enable the understanding of systematic features of the compound nucleus decay over a wide mass region (Fig. 15). Preequilibrium emission of particles in fusion reactions seems to be much more prevalent for reactions induced by α-particles or lighter ions. Nevertheless, some evidence for such effects seems to be emerging (Fig. 16). The cross sections associated with preequilibrium decay are not a major fraction of the overall reaction cross section.

B. Deep Inelastic Scattering

Deep inelastic scattering and fusion differ mainly in the degree to which the initial kinetic energy of relative motion is converted into internal degrees of freedom. The initial stages of each of these processes are probably similar. The two types of reactions are sometimes distinguished in that the deep inelastic collision results in a binary fragmentation whereas fusion need not. The sharpness of this distinction diminishes as the size of the projectile-like fragment decreases (or if the compound nucleus fissions). The deep inelastic reaction offers the possibility to probe the early and middle stages of a reaction in which frictional or viscous forces convert kinetic energy to heat; the light fragment may be thought of as the probe. Energy loss is not the only result of the nonconservative forces - angular momentum is transferred as well and enables one to distinguish different components of the frictional force (i.e. radial friction and tangential friction). The study of angular momentum transfer is of great importance for further understanding of heavy ion collisions, and a number of experimental methods have been brought to bear on this problem.

The preferential emission of charged particles in the reaction plane shows the fragments to be aligned as a result of the collision (Fig. 19). An estimate of the transferred angular momentum can be obtained through knowledge of the temperature and moment of inertia of the emitting nucleus. The angular correlation of fission fragments produced in the reaction Kr + Bi has enabled a determination of the angular momentum transfer for a heavy system (Fig. 21). The results indicate a coefficient of tangential friction larger than that used in a global set of calculations (Gr 75). The deduction of a coefficient of friction from a deep inelastic scattering measurement requires a theoretical treatment of the entire scattering orbit.

The angular momentum transfer has been deduced from measurements of the average number of γ-rays emitted. Because the γ-rays appear after particle emission (Fig. 24) corrections for the excitation energy

and angular momentum removed by particles have to be applied. In spite of these difficulties a number of features of the reaction have emerged. In one (particularly light) system $^{16}O + ^{27}Al$ evidence for fragment alignment has been obtained from the angular correlation of discrete γ-ray lines (Fig. 22). Measurements on a number of systems (Figs. 25-28) suggest that the compound system lives sufficiently long for the frictional forces to bring the system to nearly rigid rotation (sticking limit) before scission occurs. Measurements of the higher moments of the distribution of γ-rays for a deep inelastic collision reveal a broader distribution of γ-rays than is suggested by an analysis assuming similar decay mechanisms for the compound nucleus ^{75}Br and the fragments produced in the deep inelastic collision of $^{20}Ne + ^{63}Cu$ (Fig. 29).

The time scale for deep inelastic collisions can be roughly estimated on general grounds. We expect that the ejection of particles before the fragments have equilibrated or even before scission may occur if high local temperatures ($T \sim 3$-6 MeV) are produced (Fig. 30). Although the bulk of the decay process can be accounted for by equilibrium mechanisms, there is some experimental evidence for such preequilibrium processes. These measurements are still few in number and much further work is necessary. However, measurement of the angular correlation between α-particles and the projectile-like fragment (Figs. 31,33) indicates the emission of α-particles on a time scale comparable to or shorter than that of the lifetime of the compound system. In one case $^{16}O + ^{58}Ni$ the particles are ejected preferentially in the forward direction, in the other case, Kr + Au, they appear perpendicular to the direction of the separating fragments. These "preequilibrium" particles are probes for studying nuclear matter under extreme conditions of temperature.

ACKNOWLEDGEMENTS

Many people responded swiftly and generously to a request for their latest experimental results. Without their cooperation and help it would not have been possible to present such a breadth of current experimental information. (Unfortunately it was not possible because of length restrictions to include all of the interesting contributions I received.) I should like to express my thanks to Drs. J. M. Alexander, T. Cormier, B. Cujec, J. de Boer, M. Deleplanque, P. Dyer, P. Glässel, A. Gobbi, M. Lefort, F. Plasil, F. Pühlhofer, D. Sarantites, J. P. Schiffer, Z. Switkowski, K. Van Bibber, and J. P. Wurm, for information they sent me which has been incorporated in this article. Dr. Roland Dayras acted as critic in a number of stimulating conversations on the experiments described herein and is also thanked for a careful reading of the manuscript. Finally, I would especially like to thank Mrs. Christine Wallace for her help in preparing the camera-ready manuscript.

REFERENCES

Al 75) R. Albrecht, W. Dünnweber, G. Graw, H. Ho, S. G. Steadman, and J. P. Wurm, Phys. Rev. Lett. 34, 1400 (1975).

Al 77) J. M. Alexander, private communication; J. M. Miller, G. Catche, D. Logan, M. Rajagopalan, J. M. Alexander, M. Kaplan, and M. S. Zisman, work in progress.

Ar 76) M. Arnould and W. M. Howard, Nucl. Phys. A274, 295 (1976).

Ba 73) R. Bass, Phys. Letters 47B, 139 (1973); Nucl. Phys. A231, 45 (1974).

Be 76) R. R. Betts, W. A. Lanford, M. H. Mortensen, and R. L. White, Proc. Symp. on Macroscopic Features of Heavy Ion Collisions, Argonne Natl. Lab. 1976 (ANL/PHY-76-2), unpublished, p. 443.

Be 76b) M. Berlanger, M. A. Deleplanque, C. Gerschel, F. Hanappe, M. Leblanc, J. F. Mayault, C. Ngô, D. Paya, N. Perrin, J. Peter, B. Tanain, and L. Valentin, J. Phys. Lettres 37, L-323 (1976).

Bl 75) M. Blann, Ann. Rev. Nucl. Sci. 25, 123 (1975).

Bo 75) J. P. Bondorf, J. R. Huizenga, M. I. Sobel, and D. Sperber, Phys. Rev. C 11, 1265 (1975).

Bo 76) R. Boch, B. Fischer, A. Gobbi,* K. Hildenbrand, W. Kohl, V. Lynen, I. Rode, H. Stelzer, G. Auger, J. Galin, J. M. Lagrange, R. Albrecht, and B. B. Back. *Presented at the IX Masurian School in Nuclear Physics, Mikolaiki, August 1976. See also Proc. Caen Conf., p. 167 (1976).

Br 76) P. Braun-Munzinger, T. M. Cormier, and C. K. Gelbke, Phys. Rev. Lett. 37, 1582 (1976).

Br 76b) H. C. Britt, B. H. Erkkila, R. H. Stokes, H. H. Gutbrod, F. Plasil, R. L. Ferguson, and M. Blann, Phys. Rev. C 13, 1483 (1976).

Br 76c) H. C. Britt, B. H. Erkkila, P. D. Goldstone, R. H. Stokes, F. Plasil, R. L. Ferguson, and H. H. Gutbrod, Proc. Symp. on Macroscopic Features of Heavy-Ion Collisions, Argonne Natl. Lab. 1976 (ANL/PHY-76-2), unpublished, p. 491.

Ch 77) P. R. Christensen and Z. E. Switkowski, Nucl. Phys. A280, 205 (1977).

Co 74) S. Cohen, F. Plasil, W. T. Swiatecki, Ann. Phys. (N.Y.) 82, 557 (1974).

Co 76) M. Conjeaud, S. Gary, S. Harar, and J. P. Wieleckzo, European Conf. on Nuclear Physics with Heavy Ions, Caen, 1976, p. 116.

Co 76b) J. P. Coffin, P. Engelstein, and P. Wagner, Proc. European Conf. on Nuclear Physics with Heavy Ions, Caen, 1976, p. 127.

Co 77) T. M. Cormier, E. R. Cosman, A. J. Lazzasini, H. E. Wegner, J. D. Garrett, and F. Pühlhofer, Phys. Rev. C 15, 654 (1977).

Co 77b) T. M. Cormier, P. Braun-Munzinger, P. M. Cormier, J. W. Harris, and L. L. Lee, Jr., to be published in Phys. Rev. C.

Cu 76) B. Cujec and C. A. Barnes, Nucl. Phys. A266, 461 (1976).

Cu 77) B. Cujec, private communication.

Da 76) R. A. Dayras, R. G. Stokstad, Z. E. Switkowski, and R. M. Wieland, Nucl. Phys. A261, 478 (1976).

Da 76b) R. A. Dayras, R. G. Stokstad, Z. E. Switkowski, and R. M. Wieland, Nucl. Phys. A265, 153 (1976).

Da 77) R. A. Dayras, R. G. Stokstad, M. L. Halbert, D. C. Hensley, C. B. Fulmer, R. Robinson, A. H. Snell, D. G. Sarantites, and L. Westerberg, ORNL Physics Division 1976 Ann. Report.

Dy 77) P. Dyer, R. J. Puigh, R. Vandenbosch, T. D. Thomas, and M. S. Zisman, to be published (1977), private communication.

Ei 77) Y. Eisen, I. Tserruya, Y. Eyal, Z. Fraenkel, and M. Hillman, Weizmann Institute of Science Preprint WIS 77/19-Ph. See also Y. Eyal, M. Beckerman, R. Chechik, Z. Fraenkel, and H. Stocker, Phys. Rev. C 13, 1527 (1976).

Er 58) T. Ericson and V. M. Strutinski, Nucl. Phys. 8, 284 (1958).

Fo 75) W. A. Fowler, G. R. Caughlan, and B. A. Zimmerman, Ann. Rev. Astron. and Astrophys. 13, 69 (1975).

Ga 74) J. Galin, D. Guerreau, M. Lefort, and X. Tarrago, Phys. Rev. C 9, 1018 (1974).

Ga 76) J. Galin, Proc. European Conference on Nuclear Physics with Heavy Ions, Caen, 1976; J. de Physique C5-37, 83 (1976).

Gl 74, 76) D. Glas and U. Mosel, Phys. Letters 49B, 301 (1974); Nucl. Phys. A264, 268 (1976).

Gl 75) D. Glas and U. Mosel, Nucl. Phys. A275, 429 (1975).

Gl 77) P. Glässel, R. S. Simon, R. M. Diamond, R. C. Jared, I. Y. Lee, L. G. Moretto, J. O. Newton, R. Schmitt, and F. S. Stephens, Phys. Rev. Lett. 38, 331 (1977).

Go 77) J. Gomez del Campo, LILITA - A Monte-Carlo Hauser-Feshbach Computer Code, Phys. Rev. Lett. 36, 1529 (1976).

Gr 74) D. H. E. Gross and H. Kalinowski, Phys. Letters 48B, 302 (1974).

Gr 75) D. H. E. Gross, H. Kalinowski, and J. N. De in "Classical and Quantum Mechanical Aspects of Heavy-Ion Collisions," H. L. Harney, P. Braun-Munzinger and C. K. Gelbke, Eds., Lecture Notes in Physics, Vol. 33, p. 194 (Springer-Verlag) 1975.

Gr 77) D. H. E. Gross and J. Wilczynski, Phys. Letts. 67B, 1 (1977).

Ha 75) G. B. Hageman, R. Broda, B. Herskind, M. Ishihara, S. Ogaza, and H. Ryde, Nucl. Phys. A245, 166 (1975).

Ha 77) J. W. Harris, T. M. Cormier, D. F. Geesaman, L. L. Lee, Jr., R. L. McGrath, and J. P. Wurm, preprint; Proc. Symposium on Macroscopic Features of Heavy-Ion Collisions, Argonne, Vol. II, p. 609 (1976).

Hi 76) M. D. High and B. Cujec, Nucl. Phys. A259, 513 (1976).

Hi 77) M. Hillman and Y. Eyal, JULIAN - A Monte-Carlo Hauser-Feshbach Computer Code, Proc. European Conf. on Heavy Ions, Caen (1976), p. 109.

Hi 77b) M. D. High and B. Cujec, Nucl. Phys. A278, 149 (1977).

Ho 77) H. Ho, R. Albrecht, W. Dünnweber, G. Graw, S. G. Steadman, J. P. Wurm, D. Disdier, V. Rauch, and F. Scheibling, preprint. Proc. European Conf. on Nuclear Reactions with Heavy Ions, Caen, p. 159.

Hu 76) J. R. Huizenga, J. R. Birkelund, W. U. Schröder, K. L. Wolf, and V. E. Viola, Jr., Phys. Rev. Lett. 37, 885 (1976).

Ish 76) M. Ishihara, T. Numao, T. Fukada, K. Tanaka, and T. Inamura, IPCR-Cyclotron Report 35, May 1976, Proc. Argonne Symposium, 1976.

Ish 76b) M. Ishihara, K. Kamitsubo, T. Shimoda, T. Fukada, T. Motobayashi, T. Ohi, and I. Kohno, Proc. Caen Conf. Communications, p. 157.

Ko 77) S. E. Koonin, K. T. R. Davies, V. Maruhn-Rezwani, H. Feldmeier, S. J. Krieger, and J. W. Negele, Phys. Rev. C 15, 1359 (1977).

Ko 77b) B. Kohlmeyer, W. Pfeffer, and F. Pühlhofer, preprint.

Ma 73) M. Mazarakis and W. E. Stephens, Phys. Rev. C 7, 1280 (1973).

Ma 76) J. A. Maruhn, R. Y. Cusson, and R. K. Smith, Nucl. Phys. A270, 471 (1976).

Ma 77) V. Maruhn-Rezwani, K. T. R. Davies, and S. E. Koonin, Phys. Letters 67B, 134 (1977).

Mi 72) G. J. Michaud and E. W. Vogt, Phys. Rev. C 5, 350 (1972).

Mö 76) P. Möller and J. R. Nix, Nucl. Phys. A272, 502 (1976).

Mo 76) L. G. Moretto and R. Schmitt, Proc. European Conference on Nuclear Physics with Heavy Ions, Caen, 1976; J. Physique C5-37, 109 (1976).

Na 75) M. N. Namboodiri, E. T. Chulick, J. B. Natowitz, R. A. Kenefick, Phys. Rev. C 11, 401 (1975). M. N. Namboodiri, E. T. Chulick, J. B. Natowitz, Nucl. Phys. A263, 491 (1976). J. B. Natowitz, E. T. Chulick, M. N. Namboodiri, Phys. Rev. Lett. 31, 643 (1973).

Ni 65) J. R. Nix and W. J. Swiatecki, Nucl. Phys. 71, 1 (1965).

Pe 76) D. Pelte and U. Smilansky, European Conference on Nuclear Physics with Heavy Ions, Caen, 1976, p. 103.

Pe 77) N. Perrin and J. Peter, Institut de Physique Nucleaire Orsay Preprint IPNO-RC-77-02, presented at Winter School on Nuclear Physics Zakopane (Poland) 2/77.

Pl 75) F. Plasil and M. Blann, Phys. Rev. C 11, 508 (1975).

Pl 77) F. Plasil, paper presented at the Winter Meeting on Nuclear Physics, Bormio, Italy, Jan. 17-21, 1977, unpublished.

Pr 70) K. Preuss and W. Greiner, Phys. Letters 33B, 197 (1970).

Pü 75) F. Pühlhofer, W. Pfeffer, B. Kohlmeyer, and W. F. W. Schneider, Nucl. Phys. A244, 329 (1975).

Pü 77) F. Pühlhofer, Nucl. Phys. A280, 267 (1977).

Sa 76) D. G. Sarantites, J. H. Barker, M. L. Halbert, D. C. Hensley, R. A. Dayras, E. Eichler, N. R. Johnson, and S. A. Gronemeyer, Phys. Rev. C 14, 2138 (1976).

Sa 77) D. G. Sarantites, J. H. Barker, L. Westerberg, R. A. Dayras, M. L. Halbert, and D. C. Hensley, to be published.

Sc 77) J. P. Schiffer, private communication.

Sc 77b) W. U. Schröder and J. R. Huizenga, to be published in Annual Review of Nuclear Science, Vol. 27. University of Rochester preprint UR-NSRL-144.

Sp 74) H. Spinka and H. Winkler, Nucl. Phys. A233, 456 (1974).

Sp 76a) P. Sperr, S. Vigdor, Y. Eisen, W. Henning, D. G. Kovar, T. R. Ophel, and B. Zeidman, Phys. Rev. Lett. 36, 405 (1976).

Sp 76b) P. Sperr, T. H. Braid, Y. Eisen, D. G. Kovar, F. W. Prosser, J. P. Schiffer, S. L. Tabor, and S. Vigdor, Phys. Rev. Lett. 37, 321 (1976).

St 74) R. G. Stokstad, Proc. Int. Conf. on Reactions between Complex Nuclei, Nashville, Tenn., Vol. II, p. 327, North Holland Co. (1974).

St 76) R. G. Stokstad, Z. E. Switkowski, R. A. Dayras, and R. M. Wieland, Phys. Rev. Lett. 37, 888 (1976).

St 77) R. G. Stokstad, R. A. Dayras, J. Gomez del Campo, P. H. Stelson, C. Olmer, M. S. Zisman, preprint. R. G. Stokstad, J. Gomez del Campo, J. A. Biggerstaff, A. H. Snell, and P. H. Stelson, Phys. Rev. Lett. 36, 1529 (1976).

Sw 76c) Z. E. Switkowski, R. G. Stokstad, and R. M. Wieland, Nucl. Phys. A274, 202 (1976).

Sw 77a) Z. E. Switkowski, R. G. Stokstad, and R. M. Wieland, Nucl. Phys. A279, 502 (1977).

Sw 77b) Z. E. Switkowski, Shiu-Chin Wu, J. C. Overly, and C. A. Barnes, Caltech preprint LAP-157 (1976).

Tr 77) W. Trautmann, J. de Boer, W. Dünnweber, G. Graw, R. Kopp, C. Lauterbach, H. Puchta, and U. Lynen, work in progress; J. de Boer, private communication.

Va 73) R. Vandenbosch and J. R. Huizenga, Nuclear Fission, Academic Press, N.Y. (1973).

Va 77) K. Van Bibber, R. Ledoux, S. G. Steadman, F. Videbaek, G. Young, and C. Flaum, Phys. Rev. Lett. 38, 334 (1977).

Vi 76) S. Vigdor in Proc. Symp. on Macroscopic Features of Heavy Ion Collisions Argonne Nat. Lab. 1976 (ANL/PHY-76-2), unpublished, p. 95.

We 76) A. Weidinger, F. Busch, G. Gaul, W. Trautmann, and W. Zipper, Nucl. Phys. A263, 511 (1976).

Wi 73) J. Wilczynski, Physics Letters 47B, 484 (1973).

Wi 77) R. M. Wieland, R. G. Stokstad, and G. R. Satchler, private communitcation.

Wo 76) A. Wolf and E. Cheifetz, Phys. Rev. C 13, 1952 (1976).